separations

MDPI

Article

Functionalization of Sodium Magnesium Silicate Hydroxide/Sodium Magnesium Silicate Hydrate Nanostructures Using 2,3-Dihydroxybenzaldehyde as a Novel Nanocomposite for the Efficient Removal of Cd(II) and Cu(II) Ions from Aqueous Media

Asma S. Al-Wasidi [1], Maram T. Basha [2], Reem M. Alghanmi [2], Eida S. Al-Farraj [3] and Ehab A. Abdelrahman [3,4,*]

[1] Department of Chemistry, College of Science, Princess Nourah bint Abdulrahman University, P.O. Box 84428, Riyadh 11671, Saudi Arabia
[2] Department of Chemistry, College of Science, University of Jeddah, Jeddah 21589, Saudi Arabia
[3] Department of Chemistry, College of Science, Imam Mohammad Ibn Saud Islamic University (IMSIU), Riyadh 11623, Saudi Arabia
[4] Chemistry Department, Faculty of Science, Benha University, Benha 13518, Egypt
* Correspondence: eaaahmed@imamu.edu.sa or dr.ehabsaleh@yahoo.com

Abstract: Cd(II) and Cu(II) ions cause many diseases in humans. Therefore, they should be removed from water sources using simple and cost-effective adsorbents. Consequently, sodium magnesium silicate hydroxide/sodium magnesium silicate hydrate nanostructures were synthesized and functionalized using 2,3-dihydroxybenzaldehyde as a novel nanocomposite. Several instruments were used to characterize the synthetic products, such as an X-ray diffractometer (XRD), a Fourier-transform infrared spectrophotometer (FT-IR), an N_2 adsorption/desorption analyzer, a CHN elemental analyzer, an energy-dispersive X-ray spectrophotometer (EDS), and a field emission scanning electron microscope (FE-SEM). The functionalization of the nanostructures with 2,3-dihydroxybenzaldehyde led to the disappearance of the XRD peaks of the nanostructures and the presence of a broad XRD peak at $2\theta = 32^{\circ}$. In addition, the FE-SEM images revealed that the nanostructures consisted of spheres, cubes, and irregular shapes with an average grain size of 115 nm, and the nanocomposite consisted of spherical conglomerates consisting of needle-like shapes. The anticipated morphology following the functionalization of the nanostructures with 2,3-dihydroxybenzaldehyde resulted from the presence of 2,3-dihydroxybenzaldehyde on the backbones of the nanostructures. The EDS results showed that the nanostructures were composed of O, Na, Mg, and Si with weight percentages equal to 38.59%, 5.95%, 16.60%, and 38.86%, respectively. Additionally, the nanocomposite was composed of C, N, O, Na, Mg, and Si with weight percentages equal to 55.31%, 2.23%, 30.09%, 6.56%, 2.98%, and 12.83%, respectively. The synthesized nanostructures and nanocomposite samples were utilized for the efficient removal of cadmium and copper ions from aqueous media using the ion exchange and chelation adsorption procedures, respectively. Optimum conditions for removing the cadmium and copper ions were achieved at a pH, time, and temperature equal to 7.5, 80 min, and 298 K, respectively. The maximum uptake capacities of the synthesized nanostructures and nanocomposite samples toward cadmium ions were 89.44 mg/g and 155.04 mg/g, respectively, and the maximum uptake capacities of the synthesized nanostructures and nanocomposite samples toward copper ions were 103.73 mg/g and 177.94 mg/g, respectively. Moreover, the adsorption processes were exothermic, chemical, and followed the pseudo-second-order model and Langmuir equilibrium isotherm model.

Keywords: sodium magnesium silicate hydroxide; sodium magnesium silicate hydrate; nanostructures; nanocomposites; adsorption

check for updates

Citation: Al-Wasidi, A.S.; Basha, M.T.; Alghanmi, R.M.; Al-Farraj, E.S.; Abdelrahman, E.A. Functionalization of Sodium Magnesium Silicate Hydroxide/Sodium Magnesium Silicate Hydrate Nanostructures Using 2,3-Dihydroxybenzaldehyde as a Novel Nanocomposite for the Efficient Removal of Cd(II) and Cu(II) Ions from Aqueous Media. *Separations* **2023**, *10*, 88. https://doi.org/10.3390/separations10020088

Academic Editor: Victoria Samanidou

Received: 3 January 2023
Revised: 24 January 2023
Accepted: 25 January 2023
Published: 28 January 2023

Copyright: © 2023 by the authors. Licensee MDPI, Basel, Switzerland. This article is an open access article distributed under the terms and conditions of the Creative Commons Attribution (CC BY) license (https://creativecommons.org/licenses/by/4.0/).

1. Introduction

The rapid progress in industrialization has led to the presence of many heavy metals in water sources, and these pose a global threat to the environment and human health [1–3]. In addition to natural sources such as volcanic eruptions and weathering sedimentation, anthropogenic activities such as the wastewater discharged from the pigment, paint, chemical, and electroplating industries can release substantial amounts of heavy metals into the ecological environment. The metal smelting process is one of the main sources of heavy metal contamination. Heavy metal ions such as Zn(II), As(III), Cu(II), Pb(II), and Cd(II) are found in high concentrations in wastewater from the smelting process [4–6]. In terms of environmental sustainability, stringent discharge standards for industrial wastewater have been proposed. Moreover, the unregulated deposits and exhaust gases produced during the smelting process cause heavy metal contamination in groundwater and surface water due to rain leaching. Because of its known toxicity to humans, the Cd(II) ions in the effluents of various industries are regarded as one of the most hazardous pollutants. Symptoms include vomiting, nausea, diarrhea, damage to bone marrow, loss of calcium from bones, reduction in red blood cells, kidney failure, hypertension, loss of sense, and chest pain [7,8]. In addition, exposure to Cu(II) ions can cause stomach pain, headache, and eye irritation [9]. Consequently, it is of the utmost importance to develop efficient techniques for removing heavy metals from wastewater. A variety of physicochemical techniques, including flotation, precipitation, membrane processing, and adsorption, have been used to extract heavy metals ions from aqueous media [10–12]. Most of them have disadvantages, such as high operational costs, sludge production, and laborious procedures. Adsorption has been viewed as a competitive and promising approach for the extraction of heavy metals from aqueous media due to the wide availability of substances and ease of operation. The choice of adsorbent is the main factor in this approach in terms of efficiency and treatment cost [13–17]. Numerous types of adsorbents, including biochar, covalent organic frameworks, zeolites, and polymers, can effectively remove heavy metal ions from wastewater [18–21]. Due to their high surface area and the presence of hydroxyl groups on their surfaces, several studies have concentrated on the surface modification of nanomaterials using organic molecules such as humic acid, chitosan, diethylenetriaamine, thioglycolic acid, 3-bromo-5-chlorosalicylaldehyde, and 1-hydroxy-2-acetonaphthone for the simple separation of heavy metals by chelation with high adsorption capacity [13–15,22,23]. These functionalized nanomaterials have been observed to be economical, chemically stable, and environmentally safe. Therefore, it is anticipated that novel materials will be synthesized to increase the capacity adsorb heavy metal ions. The innovative aspects of the present work are as follows: (1) The simple and inexpensive synthesis of sodium magnesium silicate hydroxide/sodium magnesium silicate hydrate to form new nanostructures. (2) The facile functionalization of synthesized nanostructures using 2,3-dihydroxybenzaldehyde as a novel nanocomposite for the efficient removal of Cd(II) and Cu(II) ions from aqueous media. (3) Solving an environmental pollution problem by removing toxic metal ions in an effective, simple, and inexpensive way. Several instruments were used to characterize the synthetic products such as an aX-ray diffractometer (XRD), a Fourier-transform infrared spectrophotometer (FT-IR), an N_2 adsorption/desorption analyzer, a CHN elemental analyzer, an energy-dispersive X-ray spectrophotometer (EDS), and a field emission scanning electron microscope (FE-SEM). Factors affecting the adsorption of Cd(II) and Cu(II) ions, such as contact time, pH, concentration, and the adsorbent dose, were also studied.

2. Experimental

2.1. Chemicals

Sodium metasilicate pentahydrate ($Na_2SiO_3 \cdot 5H_2O$), magnesium nitrate hexahydrate ($Mg(NO_3)_2 \cdot 6H_2O$), 2,3-dihydroxybenzaldehyde ($C_7H_6O_3$), toluene (C_7H_8), sulfuric acid (H_2SO_4), cadmium(II) chloride monohydrate ($CdCl_2 \cdot H_2O$), copper(II) chloride dihydrate ($CuCl_2 \cdot 2H_2O$), thiourea (CH_4N_2S), nitric acid (HNO_3), hydrochloric acid (HCl), ethylenediaminetetraacetic acid disodium salt dihydrate ($C_{10}H_{14}N_2Na_2O_8 \cdot 2H_2O$), and sodium

hydroxide (NaOH) were obtained from Sigma Aldrich Company and utilized without additional chemical refining.

2.2. Synthesis

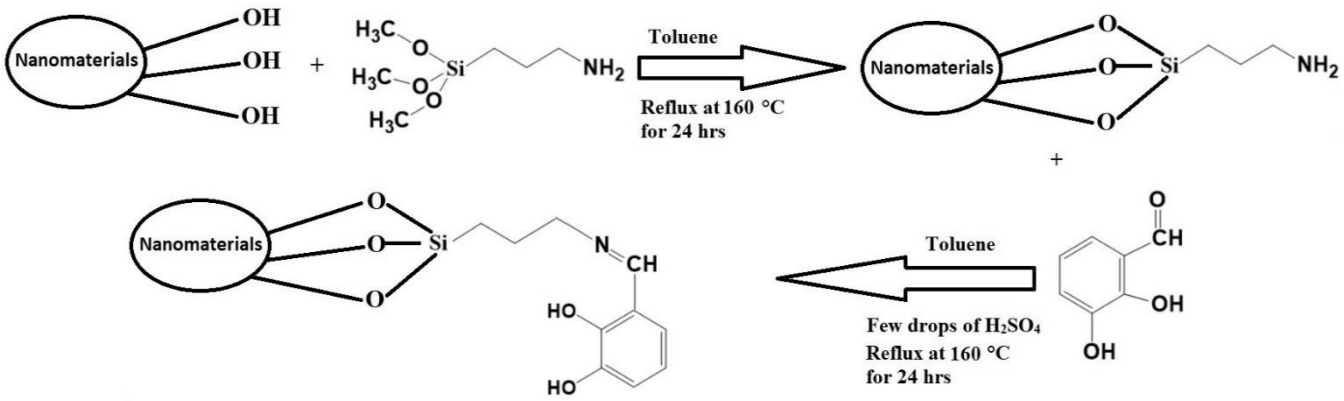
2.2.1. Synthesis of Sodium Magnesium Silicate Hydroxide/Sodium Magnesium Silicate Hydrate Nanostructures

About 8 g of $Na_2SiO_3 \cdot 5H_2O$ was dissolved in 90 mL of distilled water. Additionally, 3.65 g of $Mg(NO_3)_2 \cdot 6H_2O$ was dissolved in 90 mL of distilled water. Afterward, the magnesium nitrate solution was added dropwise to the sodium metasilicate solution with continuous stirring for 1 h. The white precipitate that formed was centrifuged, washed using distilled water, and dried at 60 °C for 6 h. The obtained nanostructures were abbreviated as F1.

2.2.2. Functionalization of Sodium Magnesium Silicate Hydroxide/Sodium Magnesium Silicate Hydrate Nanostructures Using 2,3-Dihydroxybenzaldehyde

About 4 g of sodium magnesium silicate hydroxide/sodium magnesium silicate hydrate nanostructures were stirred for 10 min in 40 mL of toluene, and then 4 mL of (3-aminopropyl)trimethoxysilane was added. Afterward, the mixture was refluxed at 160 °C for 24 h and the nanostructures modified by (3-aminopropyl)trimethoxysilane were centrifuged, washed carefully with distilled water, and dried at 60 °C. Additionally, the nanostructures modified by (3-aminopropyl)trimethoxysilane and 4 g of 2,3-dihydroxybenzaldehyde were refluxed at 160 °C for 24 h in the presence of a few drops of H_2SO_4 using 40 mL of toluene. The resulting nanocomposite was centrifuged, washed carefully with distilled water, and dried at 60 °C for 6 h. The obtained nanocomposites were abbreviated as F1S.

Scheme 1 represents the functionalization of sodium magnesium silicate hydroxide/sodium magnesium silicate hydrate nanostructures using 2,3-dihydroxybenzaldehyde.



Scheme 1. Functionalization of sodium magnesium silicate hydroxide/sodium magnesium silicate hydrate nanostructures using 2,3-dihydroxybenzaldehyde.

2.3. Instrumentation

Using a Bruker D8 Advance instrument and a CuK_α wavelength of 1.54 Å, the crystalline structures of the F1 and F1S samples were analyzed by X-ray diffraction (XRD). Using a JEOL 6510LA microscope equipped with a 10 kV accelerating voltage, the surface morphologies of the F1 and F1S samples were examined with scanning electron microscopy (SEM). Energy-dispersive X-ray analysis (EDX) was performed using an X-ray analyzer coupled to a scanning electron microscope. The pore characteristics and BET surface areas of the F1 and F1S samples were determined using N_2 adsorption/desorption analysis performed at −196 °C on a Quantachrome NOVA Touch LX2 instrument. To ensure a clean surface prior to the measurement, the samples were degassed for 12 h at 60 °C. The Fourier transform infrared (FT-IR) measurements of the F1 and F1S samples were carried out with

a Nicolet iS50 FT-IR spectrometer using KBr pellets. CHN analysis of the F1S sample was carried out by means of a 2400 PerkinElmer CHN elemental analyzer. The concentrations of the Cd(II) and Cu(II) solutions were determined using a Shimadzu AA-7000F atomic absorption spectrophotometer.

2.4. Removal of Copper and Cadmium Ions from Aqueous Media

Several factors affecting the uptake of Cu(II) and Cd(II) ions were studied by mixing a specific amount of the F1 or F1S adsorbent with Cu(II) and Cd(II) solutions and then stirring them for a specific period according to Table 1.

Table 1. Experimental conditions for the uptake of Cu(II) and Cd(II) ions using the F1 and F1S samples.

Parameter	C_o (mg/L)	V (mL)	M (g)	V_d (mL)
pH (2.5–7.5)	200	40	0.04	—
Time (10–120 min)	200	40	0.04	—
Concentration (80–280 mg/L)	—	40	0.04	—
Desorption	5	40	0.04	4
Reusability	5	40	0.04	4

C_o = initial concentration of investigated metal ions; V = volume of solution; M = amount of adsorbent; V_d = volume of desorbing solution.

The % removal (% R) of Cd(II) and Cu(II) ions was determined using Equation (1) [13].

$$\%R = \frac{C_o - C_e}{C_o} \times 100 \quad (1)$$

where C_e (mg/L) is the equilibrium concentration of the studied metal ions.

The adsorption capacity (Q, mg/g) of the F1 and F1S samples was determined using Equation (2) [13].

$$Q = (C_o - C_e) \times \frac{V}{M} \quad (2)$$

The desorption efficiency (% D) was determined using Equation (3) [13].

$$\%D = \frac{C_d \times V_d}{(C_o - C_e)V} \times 100 \quad (3)$$

where C_d (mg/L) is the concentration of the studied metal ions in the desorbing agent.

3. Results and Discussion

3.1. Characterization of the Synthesized Samples

The XRD patterns of the F1 and F1S samples are depicted in Figure 1A,B, respectively. The results indicate that the F1 sample is composed of two phases, i.e., sodium magnesium silicate hydroxide (chemical formula: $Na_2Mg_6Si_8O_{22}(OH)_2$; JCPDS No. 01-030-1215) and sodium magnesium silicate hydrate (Chemical formula: $Na_2Mg_3Si_6O_{16}{\cdot}8H_2O$; JCPDS No. 00-013-0310). The mean crystallite size of the F1 sample is 85.34 nm. Sodium magnesium silicate hydrate is responsible for the observed peaks at 2θ = 6.29° and 36.19°. In addition, the peaks found at 2θ = 19.41°, 21.81°, 29.40°, 47.84°, 53.09°, 55.50°, and 60.36° are due, respectively, to the (040), (140), (060), (500), (−202), (−323), and (−2 10 2) miller indices of sodium magnesium silicate hydroxide. After the union of the nanostructures with the 2,3-dihydroxybenzaldehyde, as suggested in Scheme 1, the peaks of the nanostructures were so strongly affected that they disappeared, while a broad peak appeared at 2θ = 32° [13–15]. This observation agrees with similar work in the literature about the functionalization of several nanomaterials, such as silica and sodium aluminum silicate hydrate,

with many organic materials, such as thioglycolic acid, 3-bromo-5-chloro-salicylaldehyde, 1-hydroxy-2-acetonaphthone, and dibenzoylmethane [13–15,24].

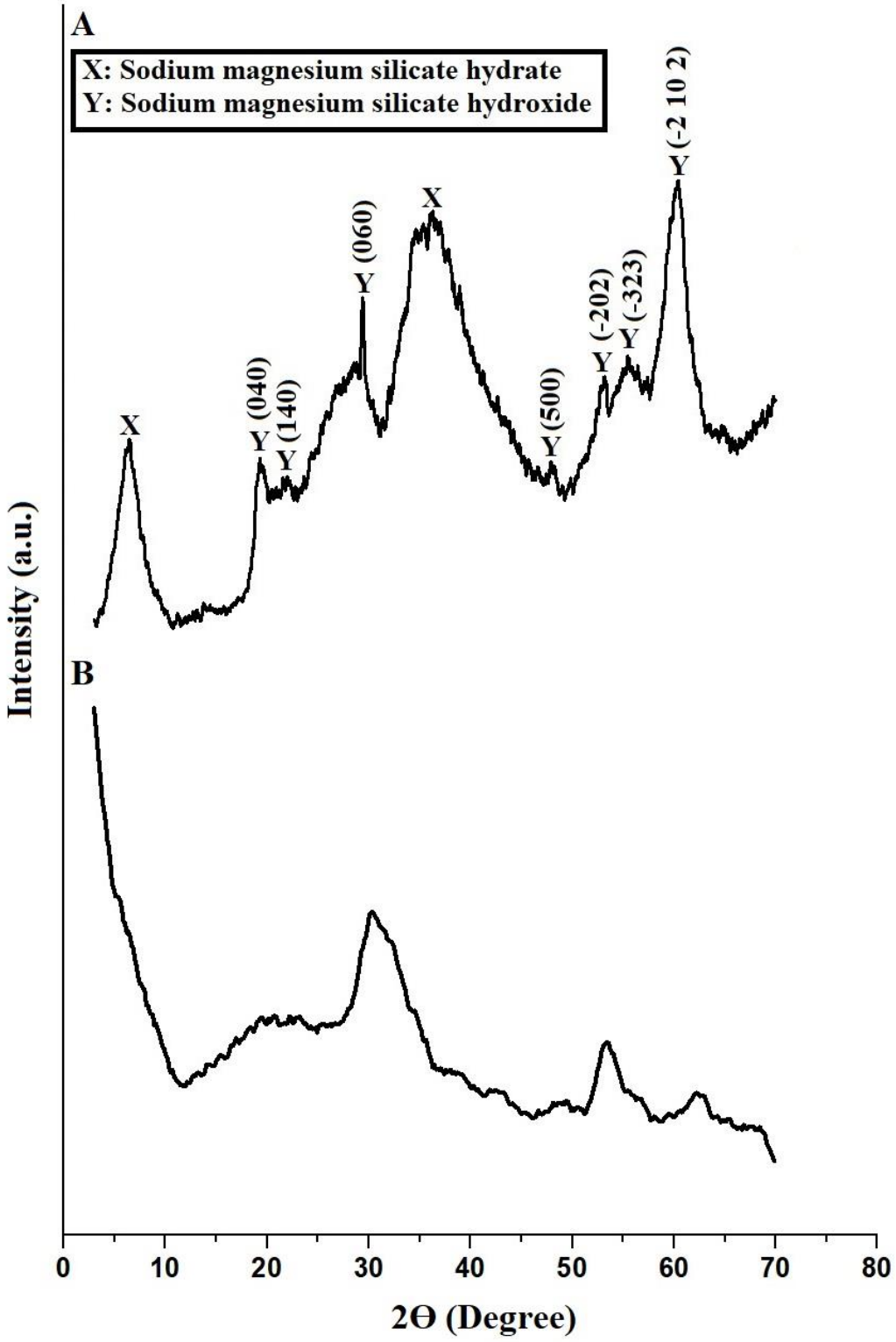


Figure 1. The XRD patterns of the F1 (nanostructures) (**A**) and F1S (nanocomposites) (**B**) samples.

The EDX patterns of the F1 and F1S products are depicted in Figure 2A,B, respectively. Furthermore, the results show that the F1 sample is composed of O, Na, Mg, and Si with weight percentages equal to 38.59%, 5.95%, 16.60%, and 38.86%, respectively, and the F1S sample is composed of C, N, O, Na, Mg, and Si with weight percentages

equal to 55.31%, 2.23%, 30.09%, 6.56%, 2.98%, and 12.83%, respectively. The union of 2,3-dihydroxybenzaldehyde with the synthesized nanostructures is responsible for the low silicon percentage and the presence of carbon (C) and nitrogen (N) in the F1S sample. The CHN elemental analysis confirmed that the F1S sample contains C, H, and N with weight percentages equal to 53.28%, 4.32%, and 1.98%, respectively, due to the functionalization of the nanostructures with 2,3-dihydroxybenzaldehyde [13–15].

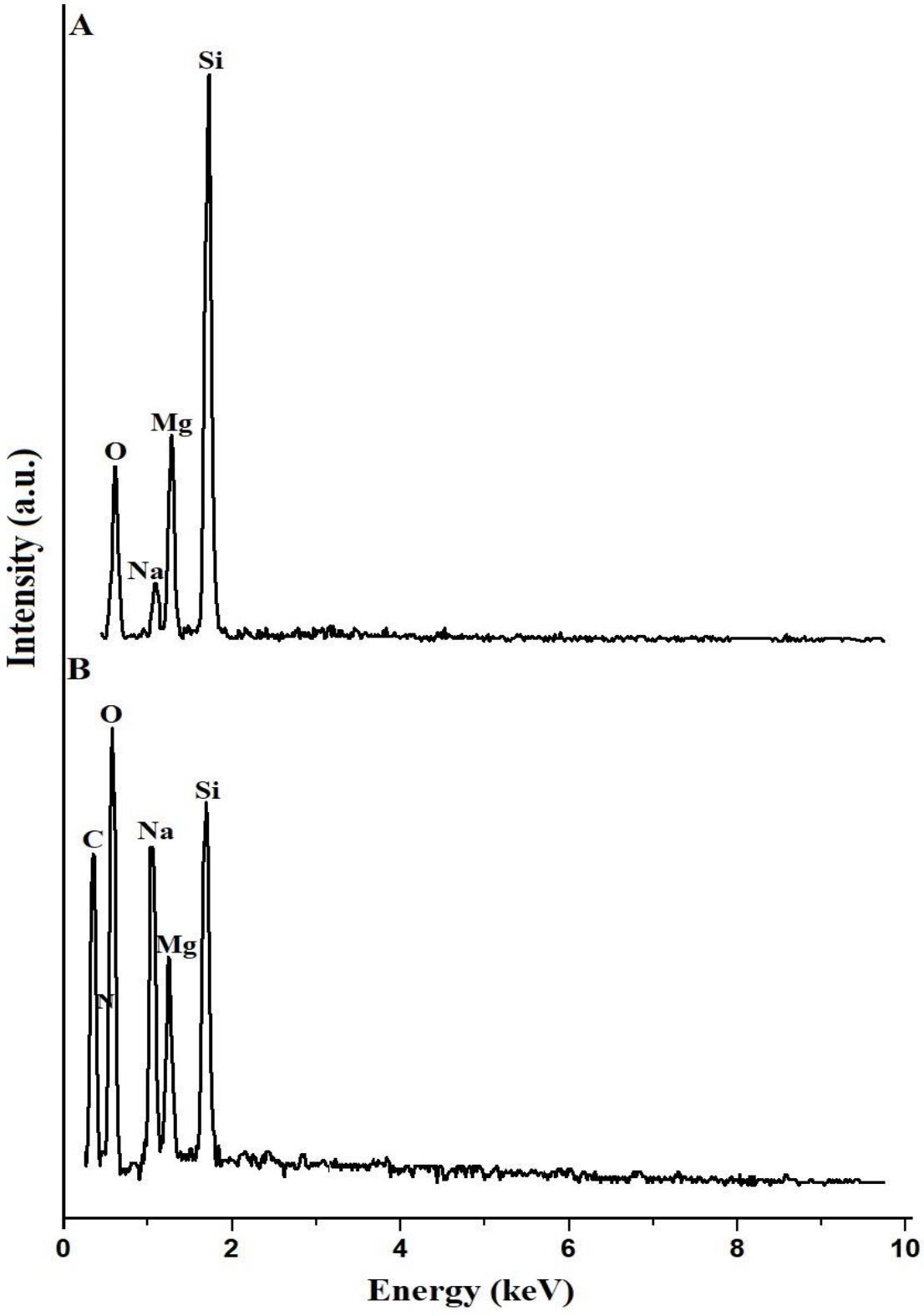


Figure 2. The EDX patterns of the F1 (nanostructures) (**A**) and F1S (nanocomposites) (**B**) samples.

The FT-IR spectra of the F1 and F1S products are depicted in Figure 3A,B, respectively. Additionally, the results reveal that the bands which were observed at 441 cm^{-1} and 524 cm^{-1} in the F1 and F1S products, respectively, are due to the bending vibrations of G-O-G (G=Si and/or Mg). The bands which appeared at 648 cm^{-1} and 642 cm^{-1} in the F1 and F1S samples, respectively, are due to the internal symmetric stretching of G-O-G. The bands which were observed at 874 cm^{-1} and 802 cm^{-1} in the F1 and F1S samples, respectively, are due to the external symmetric stretching of G-O-G. The bands which were observed at 1011 cm^{-1} and 1016 cm^{-1} in the F1 and F1S samples, respectively, are due to the internal asymmetric stretching of G-O-G. The bands which appeared at 1389 cm^{-1} and 1410 cm^{-1} in the F1 and F1S samples, respectively, are due to the external asymmetric stretching of G-O-G. The bands which appeared at 1634 cm^{-1} and 1645 cm^{-1} in the F1 and F1S products, respectively, are due to the bending vibration of O-H and/or the stretching vibration of C=N. The bands which were observed at 3448 cm^{-1} and 3437 cm^{-1} in the F1 and F1S samples, respectively, are due to the stretching vibration of O-H. The bands which were observed at 3000 cm^{-1} and 1570 cm^{-1} in the F1S sample are due to the stretching vibrations of =C-H and C=C aromatic, respectively. Finally, the bands which appeared at 1058 cm^{-1} and 1158 cm^{-1} in the F1S sample are due to the stretching vibration of C-O [13–15]. Thus, the appearance of many bands of 2,3-dihydroxybenzaldehyde as shown above confirms the successful functionalization of the nanostructures by this organic substance. This observation agrees with similar work in the literature about the functionalization of several nanomaterials, such as silica and sodium aluminum silicate hydrate, with many organic materials, such as thioglycolic acid, 3-bromo-5-chloro-salicylaldehyde, 1-hydroxy-2-acetonaphthone, and dibenzoylmethane [13–15,24].

The FE-SEM images of the F1 and F1S samples are depicted in Figure 4A,B, respectively. The results reveal that the F1 product consists of spheres, cubes, and irregular shapes with an average grain size of 115 nm. Furthermore, the F1S product consists of spherical conglomerates consisting of needle-like shapes due to the functionalization of the nanostructures with 2,3-dihydroxybenzaldehyde. The anticipated morphology following the functionalization of the nanostructures with 2,3-dihydroxybenzaldehyde results from the presence of 2,3-dihydroxybenzaldehyde on the backbones of the nanostructures, which encapsulate the nanostructures. This observation agrees with similar work in the literature about the functionalization of several nanomaterials, such as silica and sodium aluminum silicate hydrate, with many organic materials, such as thioglycolic acid, 3-bromo-5-chloro-salicylaldehyde, 1-hydroxy-2-acetonaphthone, and dibenzoylmethane [13–15,24].

The obtained N_2 adsorption/desorption isotherms of the F1 and F1S products are depicted in Figure 5A,B, respectively. The results confirm that the obtained curves are IV types [16]. Additionally, the surface properties of the F1 and F1S samples, such as BET surface area, total pore volume, and average pore size, are shown in Table 2. Since the average pore size is greater than 2, the F1 and F1S samples are mesoporous. Furthermore, the BET surface area and total pore volume decreased as a result of the functionalization of the nanostructures with 2,3-dihydroxybenzaldehyde. The anticipated decline in the surface area following the functionalization of the nanostructures with 2,3-dihydroxybenzaldehyde is a result of the presence of 2,3-dihydroxybenzaldehyde on the backbones of the nanostructures, which prevent nitrogen gas from entering the pores of the nanostructures during the BET method. This observation agrees with similar work in the literature about the functionalization of several nanomaterials, such as silica and sodium aluminum silicate hydrate, with many organic materials, such as thioglycolic acid, 3-bromo-5-chloro-salicylaldehyde, 1-hydroxy-2-acetonaphthone, and dibenzoylmethane [13–15,24].

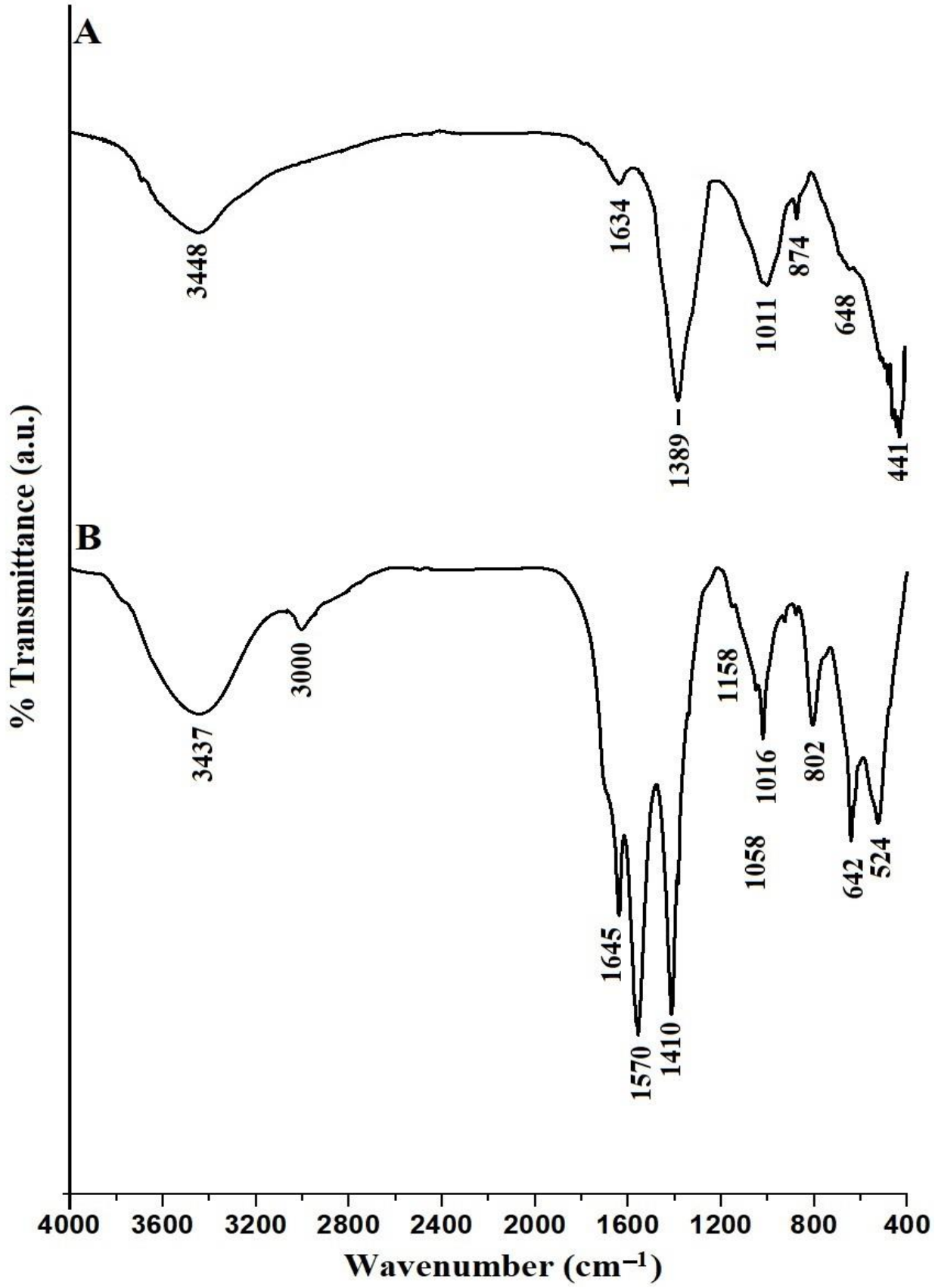


Figure 3. The FT-IR spectra of the F1 (nanostructures) (**A**) and F1S (nanocomposites) (**B**) samples.

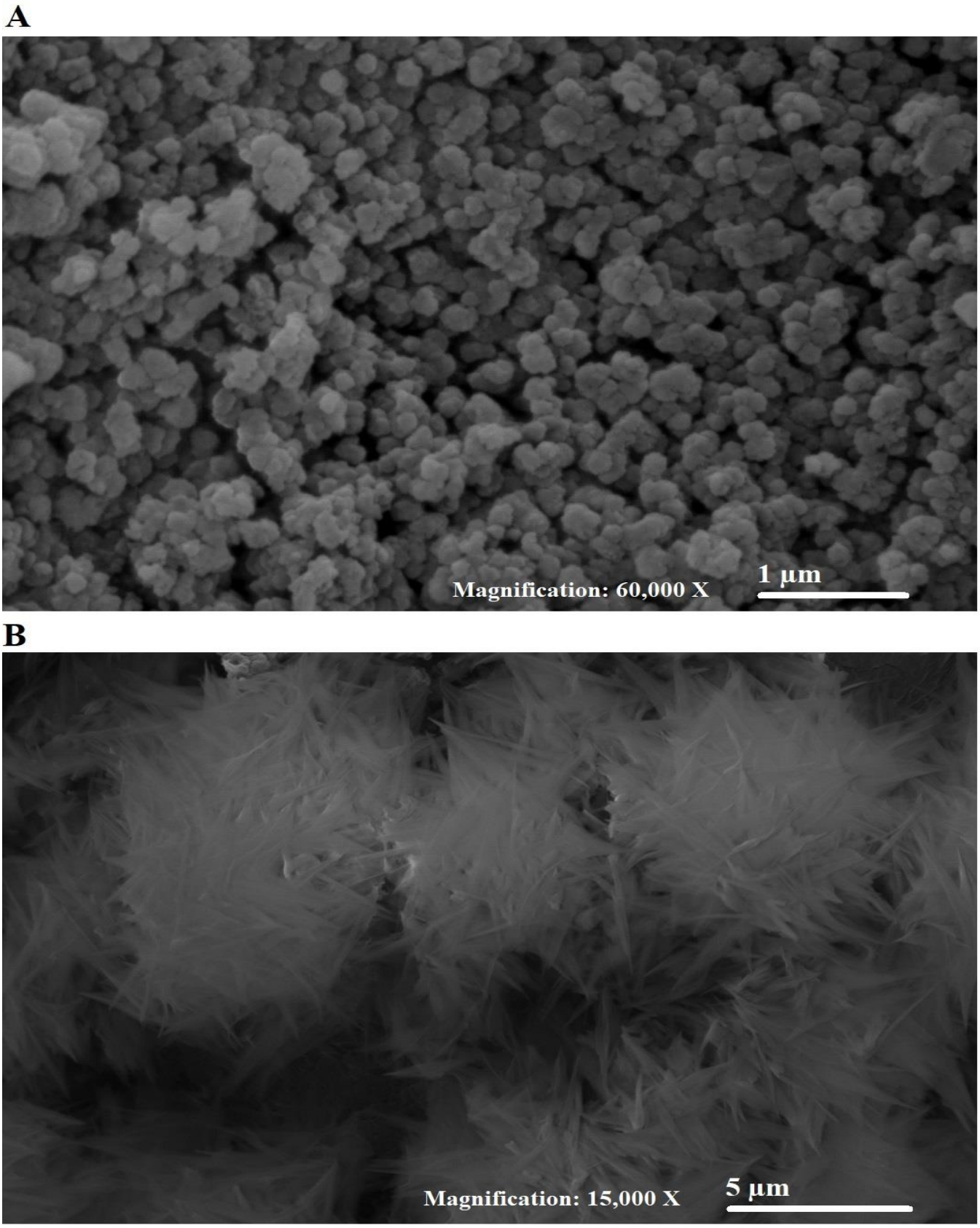


Figure 4. The FE-SEM images of the F1 (nanostructures) (**A**) and F1S (nanocomposites) (**B**) samples.

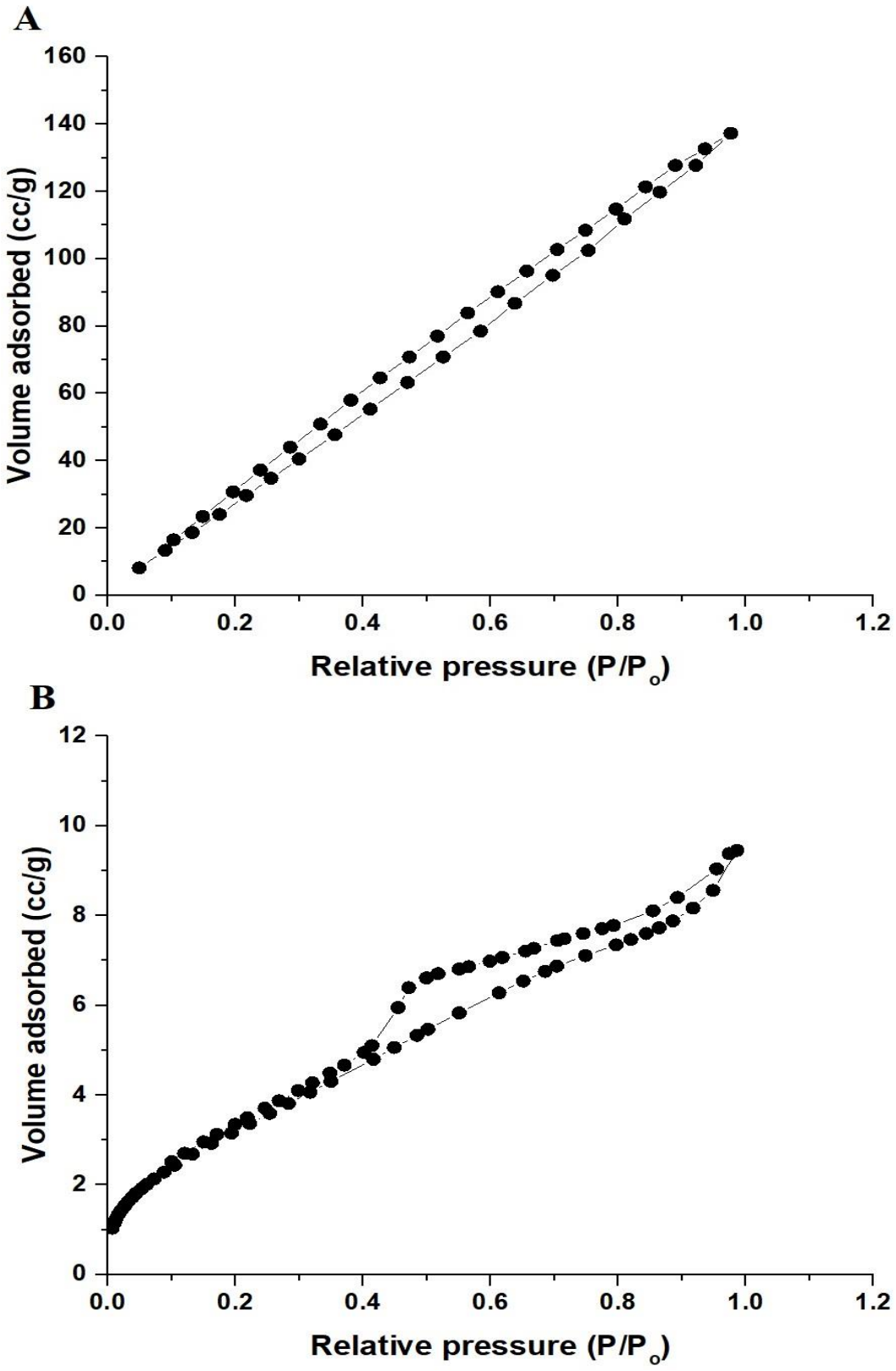


Figure 5. The N_2 adsorption/desorption isotherms of the F1 (nanostructures) (**A**) and F1S (nanocomposites) (**B**) samples.

Table 2. The BET surface area, total pore volume, and average pore size of the F1 and F1S samples.

Surface Properties	Sample	
	F1	**F1S**
BET surface area (m^2/g)	199.89	12.95
Total pore volume (cc/g)	0.2126	0.0172
Average pore size (nm)	2.1275	2.214

3.2. Removal of Cd(II) and Cu(II) Ions

3.2.1. Effect of pH

The pH plays a crucial role in the solid-phase extraction of heavy metals. A pH range of 2.5–7.5 was used to investigate the effect of pH on the % removal of cadmium and copper ions as well as the uptake capacity of the F1 and F1S samples, as is shown in Figure 6A,B, respectively. The results establish that the adsorption capacity of the F1 and F1S products, or the % removal of cadmium and copper ions, increased as the pH value increased from 2.5 to 7.5. Hence, pH 7.5 was nominated as the best value for all the experiments. At pH 7.5, the % removal of cadmium ions exploiting the F1 and F1S samples was 39.83% and 74.86%, respectively. Additionally, the uptake capacity of the F1 and F1S samples toward cadmium ions was 79.66 mg/g and 149.72 mg/g, respectively. At pH 7.5, the % removal of copper ions using the F1 and F1S samples was 50% and 85.49%, respectively. Furthermore, the uptake capacity of the F1 and F1S samples toward copper ions was 100 mg/g and 170.98 mg/g, respectively. As is shown in Scheme 2, the % removal or adsorption capacity of the F1 and F1S adsorbents decreases in an acidic medium because the adsorbents were surrounded by positive hydrogen ions (H^+), which repel the cadmium or copper ions. On the other hand, the % removal or adsorption capacity of the F1 and F1S adsorbents increases in a basic medium because the adsorbents were surrounded by negative hydroxide ions (OH^-), which attract the cadmium or copper ions.

3.2.2. Effect of Time

The contact time plays a crucial role in the solid-phase extraction of heavy metals. A contact time range of 10–120 min was used to investigate the effect of time on the % removal of cadmium and copper ions as well as the adsorption capacity of the F1 and F1S samples, as is shown in Figure 7A,B, respectively. The results establish that the adsorption capacity of the F1 and F1S samples, or the % removal of cadmium and copper ions, increased as the time value increased from 10 min to 80 min. Additionally, when the contact time was increased from 80 min to 120 min, the % removal of the studied metal ions, or adsorption capacity of the F1 and F1S samples, was not significantly affected due to the saturation of active centers. Therefore, a time of 80 min was chosen as the optimal time for all the experiments. At 80 min, the % removal of cadmium ions using the F1 and F1S samples was 40% and 74%, respectively. Furthermore, the capacity of the F1 and F1S samples to adsorb cadmium ions was 80 mg/g and 148 mg/g, respectively. At 80 min, the % removal of copper ions using the F1 and F1S samples was 50% and 86%, respectively. Additionally, the uptake capacity of the F1 and F1S samples toward copper ions was 100 mg/g and 172 mg/g, respectively. The obtained results were examined using the pseudo-first-order and pseudo-second-order kinetic models as clarified in Equations (4) and (5), respectively [24].

$$\log(Q_e - Q_t) = \log Q_e - \frac{k_1}{2.303}t \quad (4)$$

$$\frac{t}{Q_t} = \frac{1}{k_2 Q_e^2} + \frac{1}{Q_e}t \quad (5)$$

where, Q_t (mg/g) is the quantity of cadmium or copper ions adsorbed at time t (min), Q_e (mg/g) is the adsorption capacity of the F1 and F1S samples at equilibrium, k_1 (1/min) is the rate constant of the pseudo-first-order model, and k_2 (g/mg.min) is the rate constant of

the pseudo-second-order model. Figure 8A,B represents the plots of log $(Q_e - Q_t)$ and t/Q_t versus t, respectively. Table 3 contains the constants of the pseudo-first-order and pseudo-second-order kinetic models. The results follow the pseudo-second-order model more than the pseudo-first-order model because of the large value of the pseudo-second-order coefficient of determination (R^2) compared with its counterpart in the pseudo-first-order model.

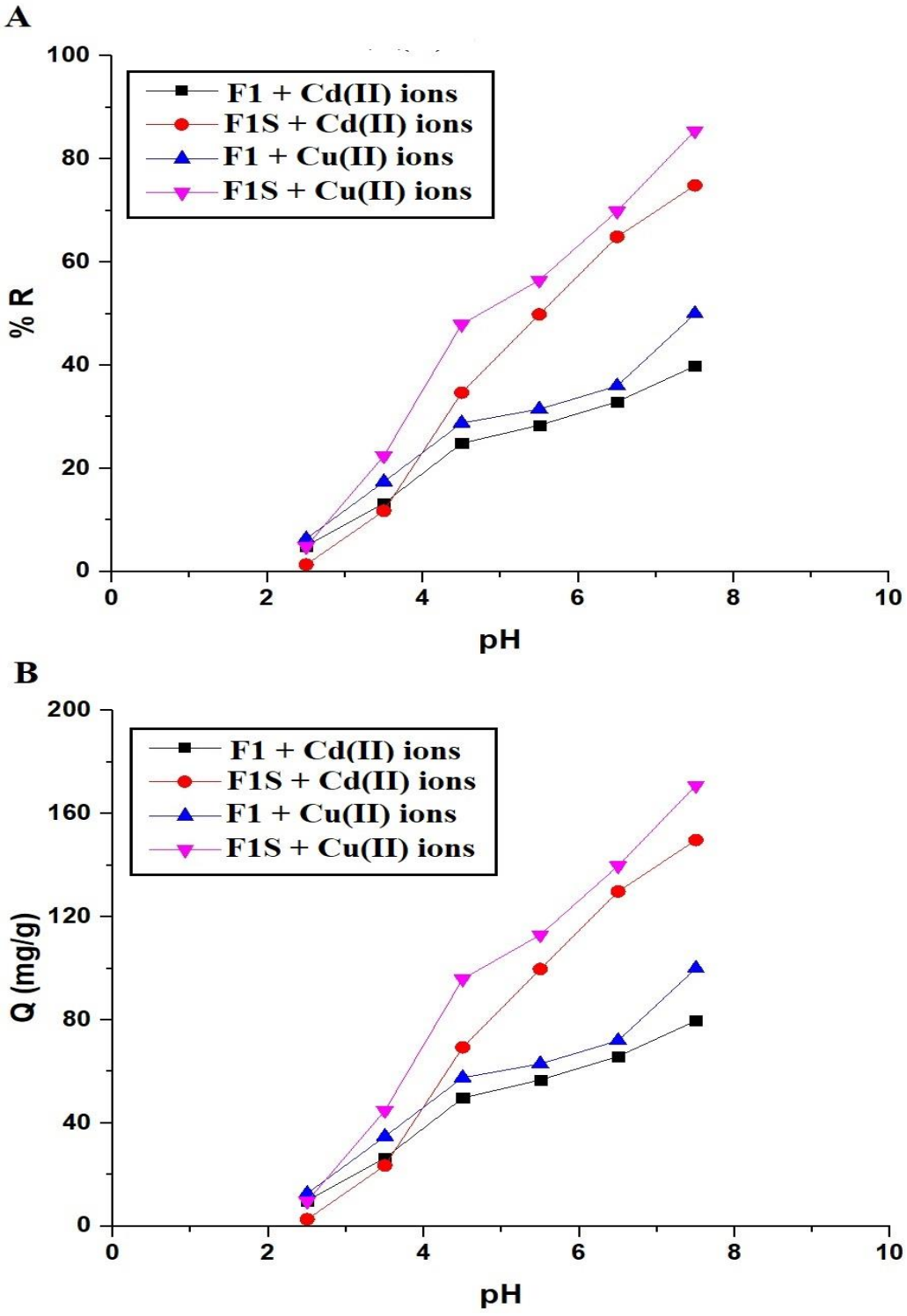
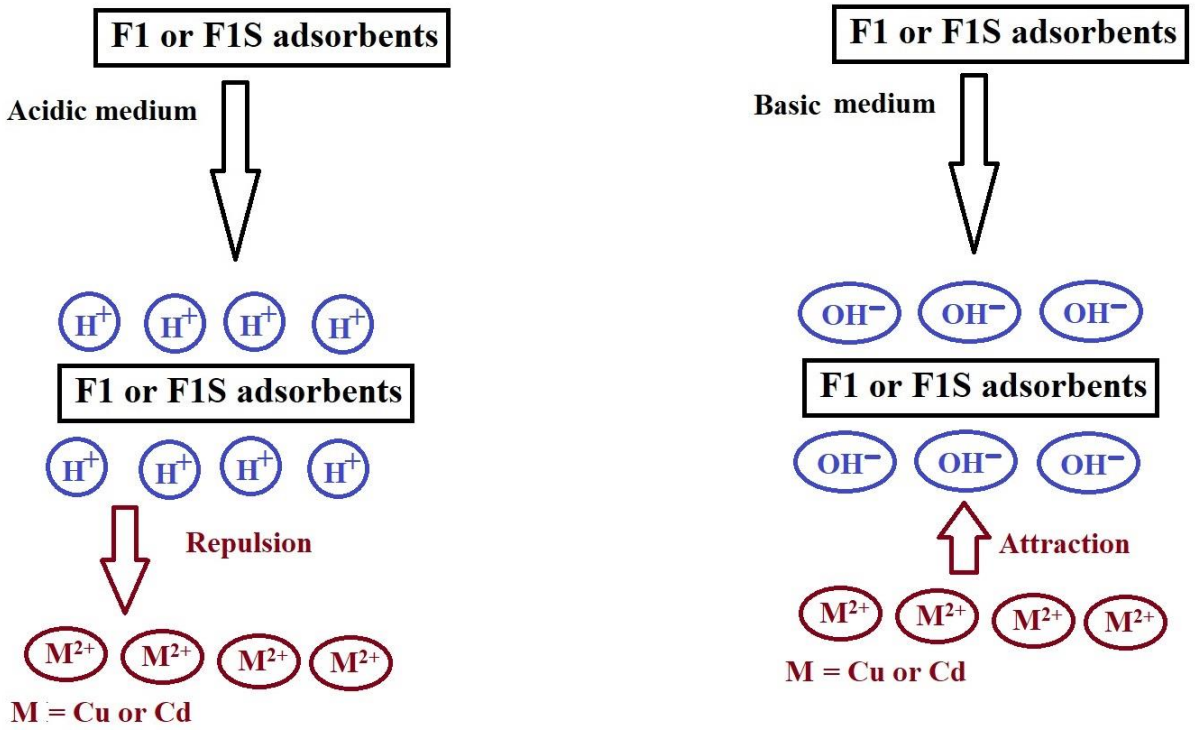


Figure 6. The effect of pH on the % removal of copper and cadmium ions (**A**) and the adsorption capacity of the F1 and F1S samples (**B**). Experimental conditions: concentration = 200 mg/L, volume = 40 mL, amount of adsorbent = 0.04 g, and time = 180 min.



Scheme 2. The effect of pH on the removal of cadmium and copper ions using the F1 and F1S adsorbents.

3.2.3. Effect of Temperature

The temperature plays a crucial role in the solid-phase extraction of heavy metals. An adsorption temperature range of 298–328 K was used to investigate the effect of temperature on the % removal of cadmium and copper ions as well as the uptake capacity of the F1 and F1S samples, as is shown in Figure 9A,B, respectively. The results establish that the adsorption capacity of the F1 and F1S products, or the % removal of cadmium and copper ions, decreased as the temperature value increased from 298 K to 328 K. At 298 K, the % removal of cadmium ions using the F1 and F1S samples was 40% and 74%, respectively. At 328 K, the % removal of cadmium ions using the F1 and F1S samples was 10.89% and 34.86%, respectively. At 298 K, the capacity of the F1 and F1S samples to adsorb cadmium ions was 80 mg/g and 148 mg/g, respectively. At 328 K, the capacity of the F1 and F1S samples to adsorb cadmium ions was 21.77 mg/g and 69.72 mg/g, respectively. At 298 K, the % removal of copper ions using the F1 and F1S samples was 50% and 86%, respectively. At 328 K, the % removal of copper ions using the F1 and F1S samples was 17.04% and 57%, respectively. At 298 K, the capacity of the F1 and F1S samples to adsorb copper ions was 100 mg/g and 172 mg/g, respectively. At 328 K, the capacity of the F1 and F1S samples to adsorb copper ions was 34.07 mg/g and 114 mg/g, respectively. As the temperature rises, cadmium and copper ions are liberated from the adsorbent and returned to the solution, speeding up the desorption process and lowering the percentage removal or adsorption capacity. Thus, a temperature of 298 K was select as the best value for all the experiments. The thermodynamic parameters for the adsorption process of cadmium and copper ions can be obtained by calculating the change in entropy (ΔS°, kJ/mol kelvin), the change in free energy (ΔG°, kJ/mol), and the change in enthalpy (ΔH°, kJ/mol) using Equations (6)–(8) and Figure 10 [24].

$$lnK_d = \frac{\Delta S^{\circ}}{R} - \frac{\Delta H^{\circ}}{RT} \quad (6)$$

$$\Delta G^{\circ} = \Delta H^{\circ} - T\Delta S^{\circ} \quad (7)$$

$$K_d = \frac{Q_e}{C_e} \quad (8)$$

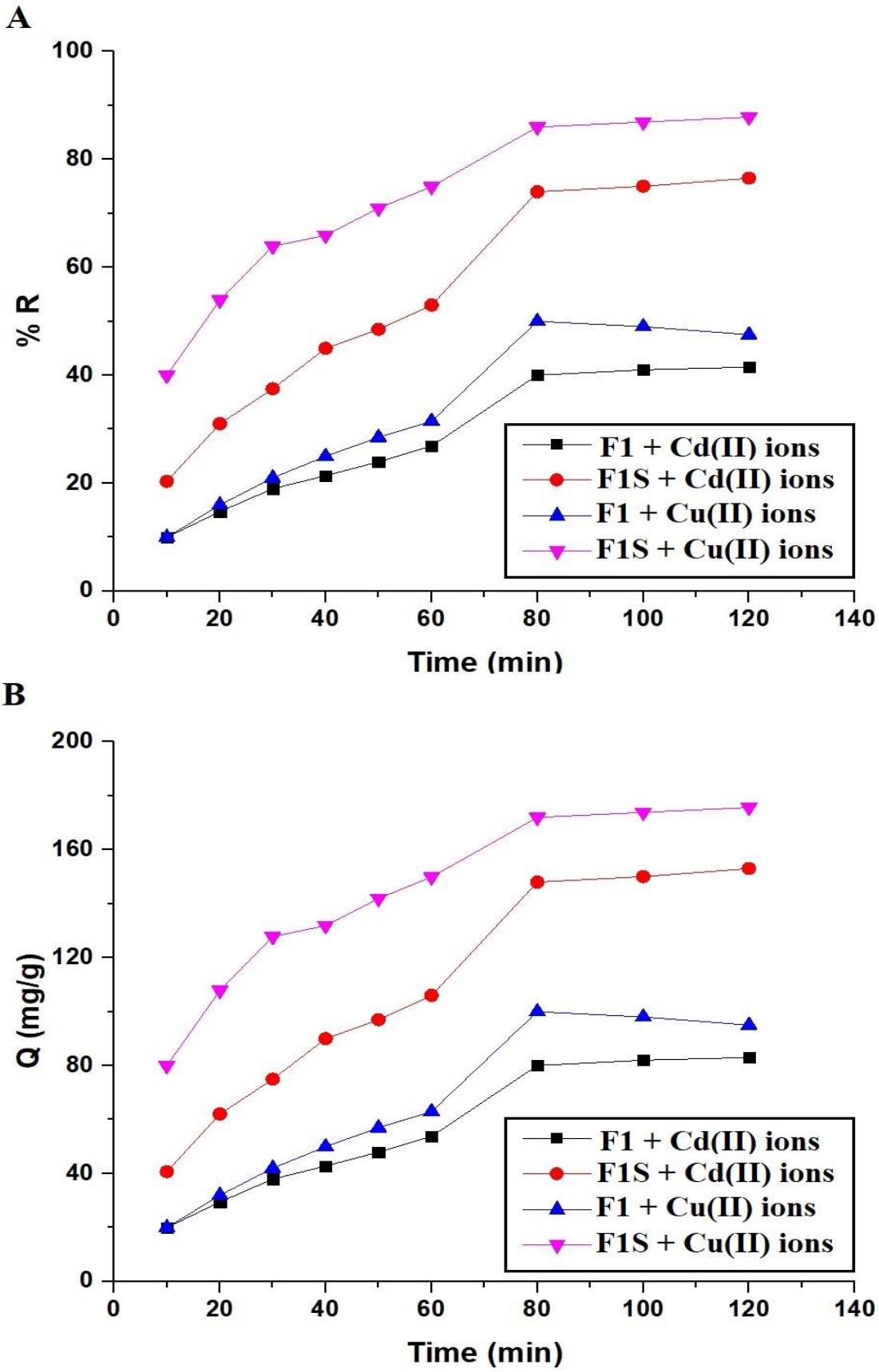


Figure 7. The effect of contact time on the % removal of copper and cadmium ions (**A**) and the adsorption capacity of the F1 and F1S samples (**B**). Experimental conditions: concentration = 200 mg/L, volume = 40 mL, amount of adsorbent = 0.04 g, and pH = 7.5.

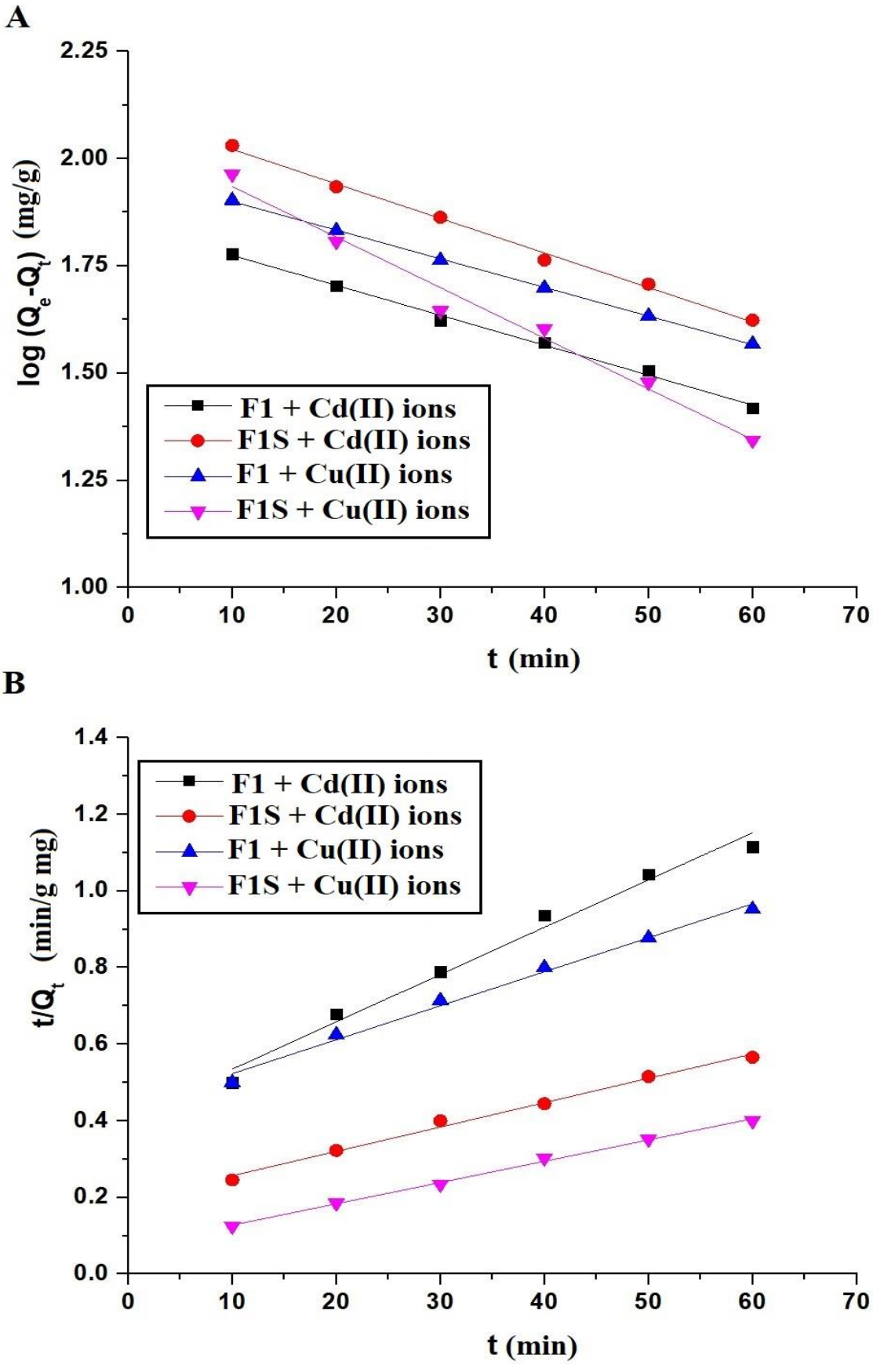


Figure 8. The plots of log $(Q_e - Q_t)$ (**A**) and t/Q_t (**B**) versus t for the removal of copper and cadmium ions using the F1 and F1S samples.

Table 3. The constants of the pseudo-first-order and pseudo-second-order kinetic models for the removal of copper and cadmium ions using the F1 and F1S samples.

Conditions	Q_e (mg/g)		Constants		R^2	
	Pseudo-First-Order	Pseudo-Second-Order	k_1 (1/min)	k_2 (g/mg·min)	Pseudo-First-Order	Pseudo-Second-Order
F1 + Cd(II) ions	69.86	81.04	0.0161	0.00037	0.9809	0.9948
F1S + Cd(II) ions	126.52	157.23	0.0185	0.00021	0.9914	0.9946
F1 + Cu(II) ions	92.66	112.74	0.0154	0.00018	0.9890	0.9996
F1S + Cu(II) ions	113.02	179.86	0.0272	0.00043	0.9771	0.9967

T (K) is the adsorption temperature, K_d (L/g) is the distribution constant, and R (kJ/mol kelvin) is the gas constant. Table 4 contains the thermodynamic constants. The adsorption processes of copper and cadmium ions are exothermic and chemical because the change in enthalpies is negative and greater than 40 kJ/mol. Additionally, the negative values of the change in free energy confirmed the spontaneous nature of the adsorption processes. Furthermore, positive values of change in entropy indicate greater randomization at the solid/solution interface following the adsorption of the cadmium and copper ions by the F1 and F1S samples.

Table 4. The thermodynamic constants for the removal of cadmium and copper ions using the F1 and F1S samples.

Conditions	ΔH° (kJ/mol)	ΔS° (kJ/mol Kelvin)	ΔG° (kJ/mol)			
			298	308	318	328
F1 + Cd(II) ions	−45.47	0.1555	−91.79	−93.35	−94.91	−96.46
F1S + Cd(II) ions	−44.32	0.1399	−86.01	−87.40	−88.80	−90.20
F1 + Cu(II) ions	−43.00	0.1444	−86.03	−87.47	−88.91	−90.36
F1S + Cu(II) ions	−42.39	0.1267	−80.16	−81.42	−82.69	−83.96

3.2.4. Effect of Concentration

The initial concentration of metal ions plays a crucial role in the solid-phase extraction of heavy metals. A concentration range of 80–280 mg/L was used to investigate the effect of concentration on the % removal of cadmium and copper ions as well as the uptake capacity of the F1 and F1S samples, as is shown in Figure 11A,B, respectively. The results establish that the adsorption capacity of the F1 and F1S products increased and the % removal of cadmium and copper ions decreased as the concentration value increased from 80 mg/L to 280 mg/L. The obtained results were examined using the Langmuir and Freundlich equilibrium isotherms as clarified in Equations (9) and (10), respectively [24].

$$\frac{C_e}{Q_e} = \frac{1}{K_L Q_m} + \frac{C_e}{Q_m} \quad (9)$$

$$lnQ_e = lnK_F + \frac{1}{n} lnC_e \quad (10)$$

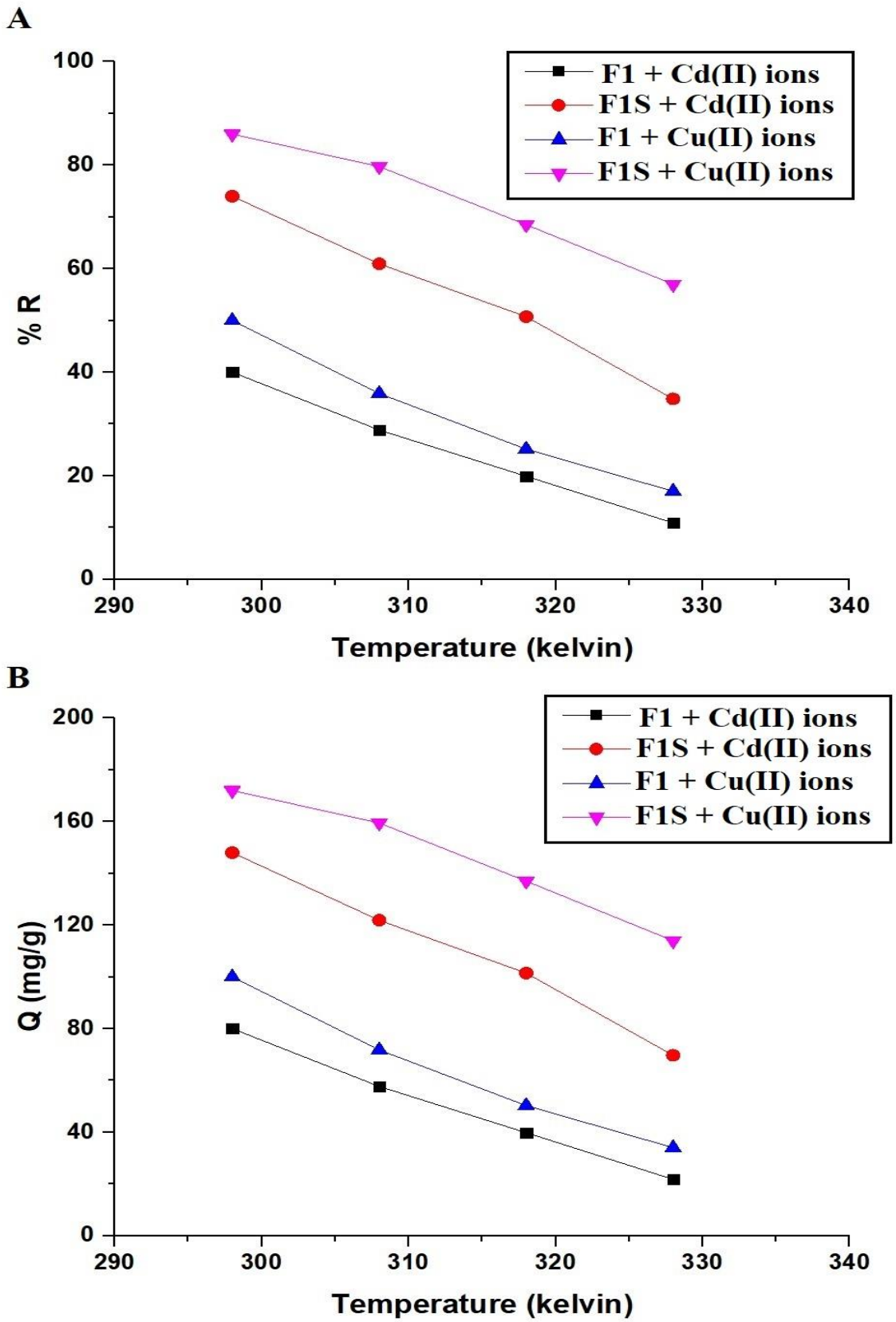


Figure 9. The effect of adsorption temperature on the % removal of copper and cadmium ions (**A**) and the uptake capacity of the F1 and F1S samples (**B**). Experimental conditions: concentration = 200 mg/L, volume = 40 mL, pH = 7.5, amount of adsorbent = 0.04 g, and time = 80 min.

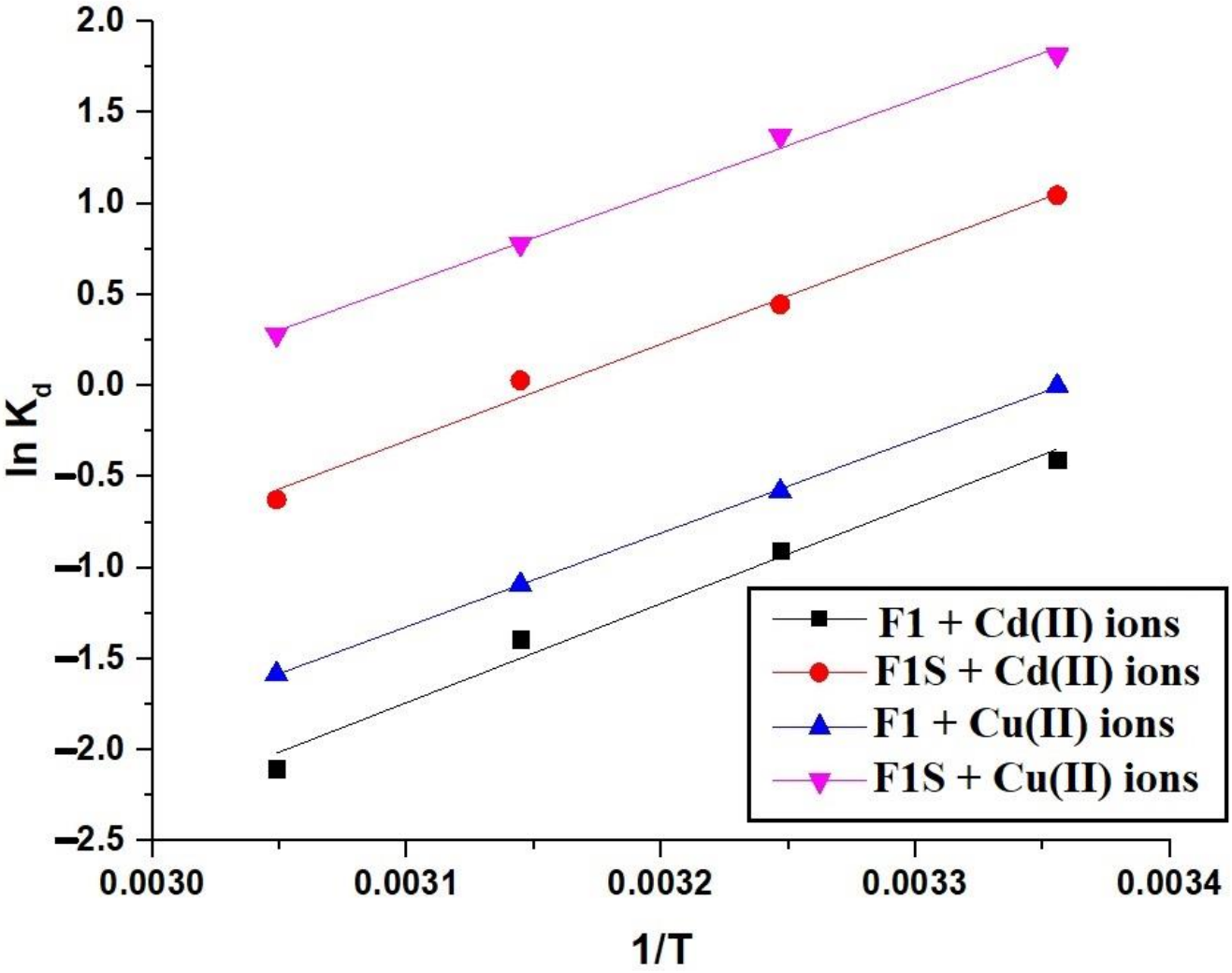


Figure 10. The plots of lnK_d versus $1/T$ for the removal of cadmium and copper ions using the F1 and F1S samples.

Q_m (mg/g) and K_L (L/mg) are the maximum adsorption capacity and constant of the Langmuir isotherm, respectively, and $1/n$ and K_F (mg/g)(L/mg)$^{1/n}$ are the heterogeneity constant and constant of the Freundlich isotherm, respectively.

Figure 12A represents the plots of C_e/Q_e versus C_e. Figure 12B represents the plots of $ln\ Q_e$ versus $ln\ C_e$. Table 5 contains the constants of the Langmuir and Freundlich equilibrium isotherms. The results follow the Langmuir isotherm more than the Freundlich because of the large value of the Langmuir coefficient of determination (R^2) compared with its counterpart in the Freundlich. Additionally, the maximum uptake capacity of the F1 and F1S samples toward cadmium ions was 89.44 mg/g and 155.04 mg/g, respectively, and the maximum uptake capacity of the F1 and F1S samples toward copper ions was 103.73 mg/g and 177.94 mg/g, respectively.

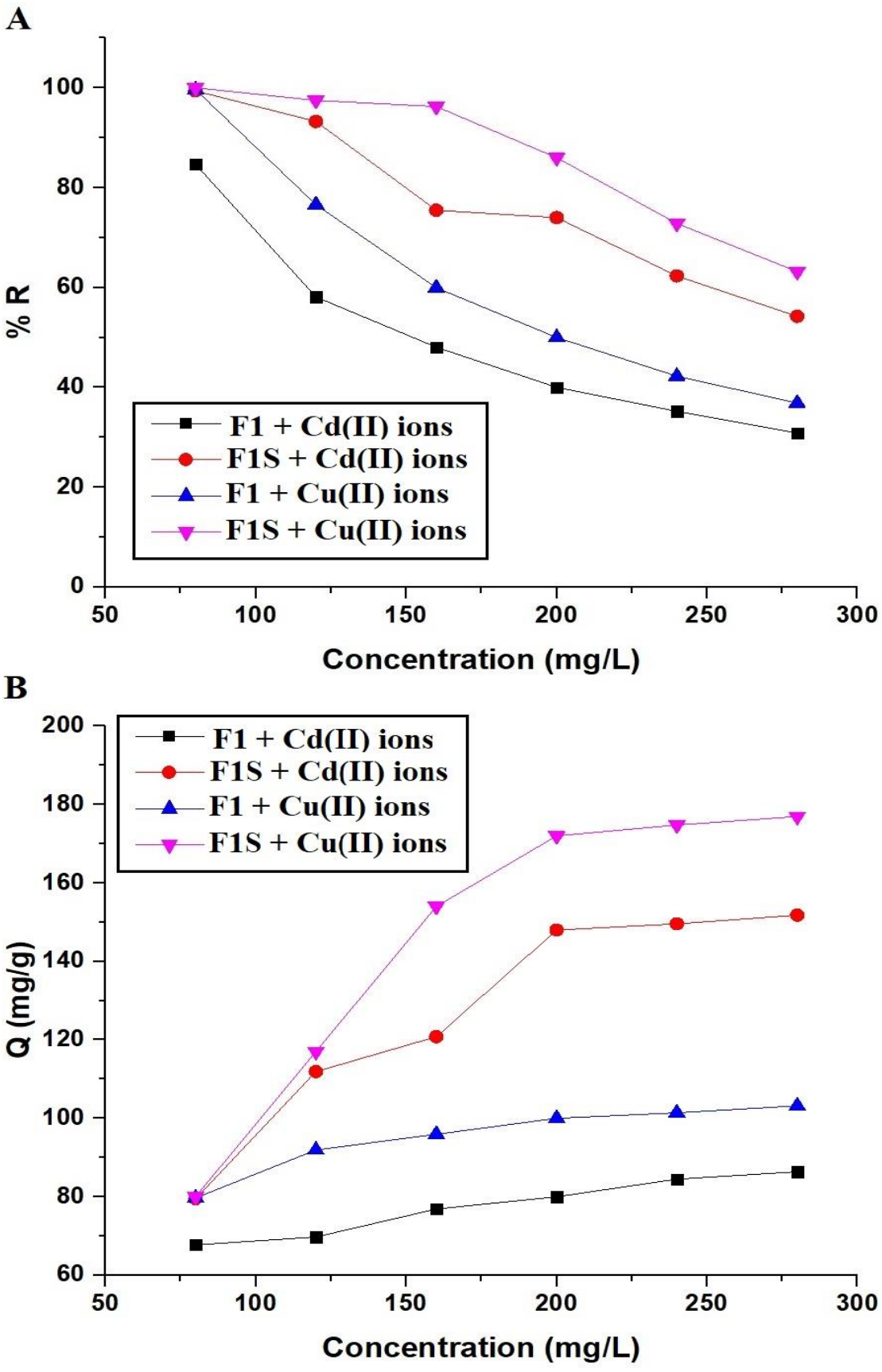


Figure 11. The effect of initial concentration of copper and cadmium ions on the % removal (**A**) and the adsorption capacity of the F1 and F1S samples (**B**). Experimental conditions: volume = 40 mL, pH = 7.5, temperature= 298 K, amount of adsorbent = 0.04 g, and time = 80 min.

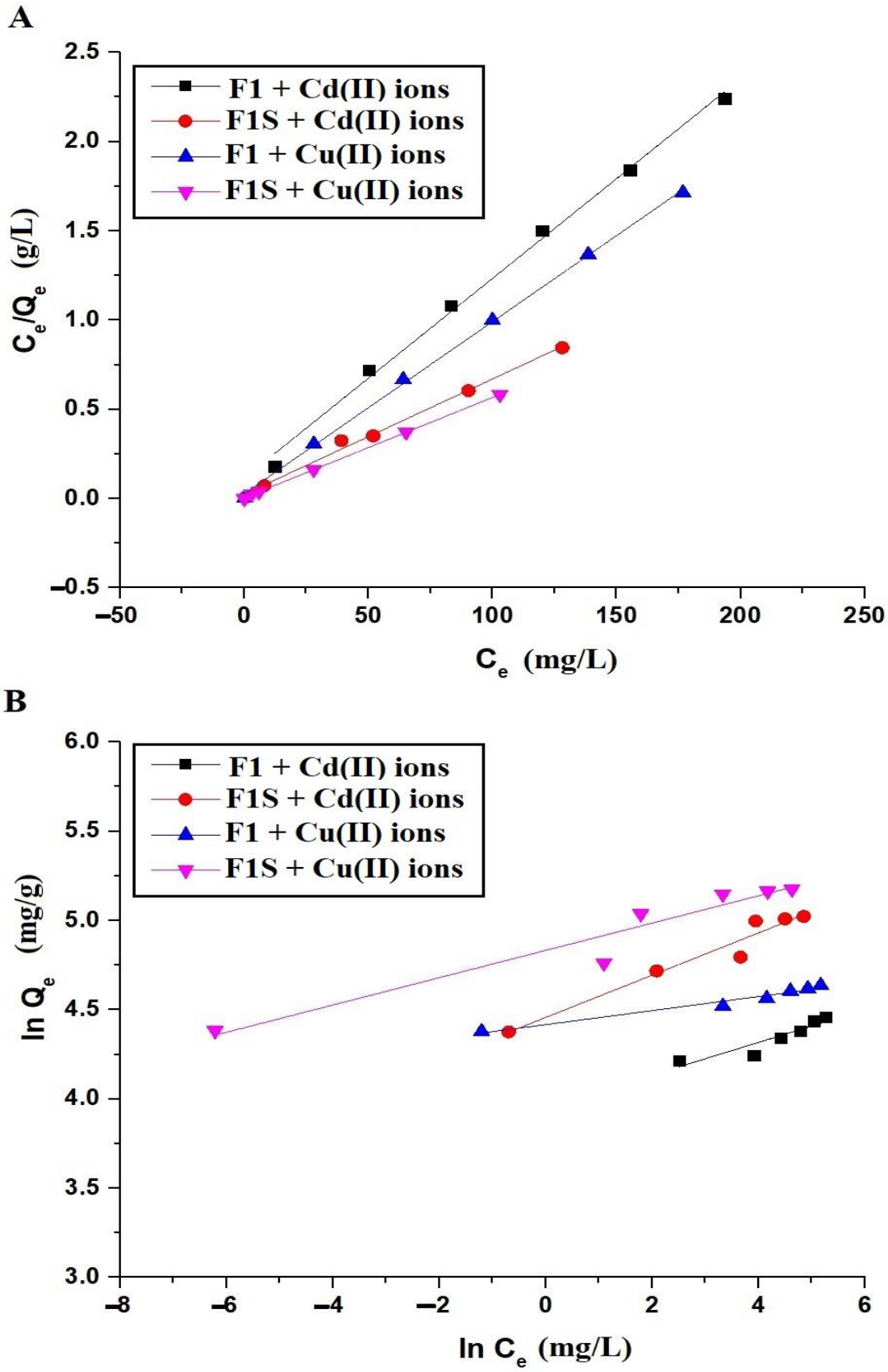


Figure 12. The Langmuir (**A**) and Freundlich (**B**) equilibrium isotherms for the removal of cadmium and copper ions using the F1 and F1S samples.

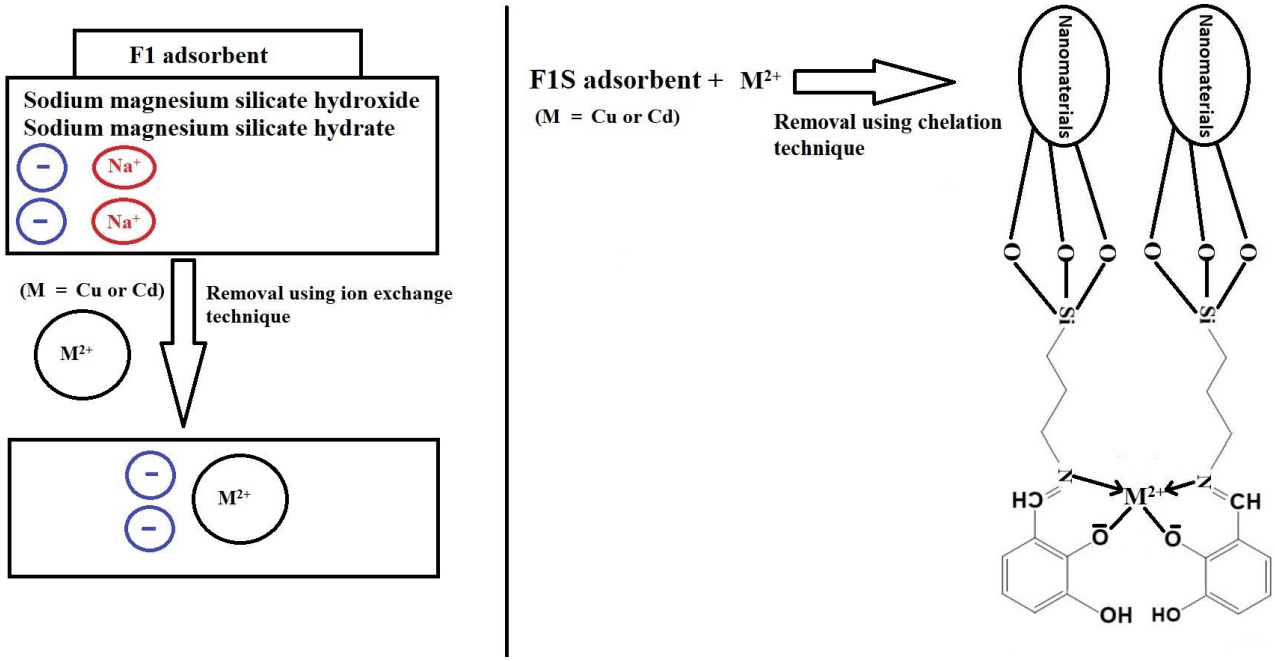
Table 5. The calculated constants of the Langmuir and Freundlich equilibrium isotherms for the removal of cadmium and copper ions using the F1 and F1S samples.

Conditions	Langmuir			Freundlich		
	Q_m (mg/g)	K_L (L/mg)	R^2	Q_m (mg/g)	K_F (mg/g)(L/mg)$^{1/n}$	R^2
F1 + Cd(II) ions	89.44	0.0969	0.9948	84.42	51.98	0.8270
F1S + Cd(II) ions	155.04	0.2605	0.9929	161.37	86.21	0.9396
F1 + Cu(II) ions	103.73	0.3562	0.9989	101.95	82.79	0.9598
F1S + Cu(II) ions	177.94	1.124	0.9998	188.15	125.49	0.9180

The % removal of the studied metal ions using the F1 and F1S samples was compared with that of many adsorbents in aforementioned studies, such as chitosan/$MnFe_2O_4$ composite, dithiocarbamate/Fe_3O_4/reduced graphene oxide composite, FAU zeolite, calcium titanate, silver/multiwalled carbon nanotubes, and guanyl-modified cellulose, as is clarified in Table 6 [25–30]. The results prove the adsorption superiority of the F1 and F1S samples over these other adsorbents. The synthesized adsorbents had the highest adsorption capacity, which made them superior compared with other adsorbents in removing Cd(II) and Cu(II) ions. The reason for this is that the F1S adsorbent can undertake ion exchange with Cd(II) or Cu(II) ions and form 6-membered ring chelates with Cd(II) and Cu(II) ions as a result of the presence of C=N and OH groups, as is shown in Scheme 3. Figure 13A,B represents the EDX patterns of the Cu(II)–F1S and Cd(II)–F1S, respectively. The success of the ion exchange and chelation mechanisms of the F1S sample with Cu(II) ions is evident through the disappearance of sodium and the appearance of copper at 0.96 eV and 7.85 eV, as is shown in Figure 13A. The success of the ion exchange and chelation mechanisms of the F1S sample with Cd(II) ions is evident through the disappearance of sodium and the appearance of cadmium at 3.04 eV, as is shown in Figure 13B. Figure 14A,B represents the FT-IR spectra of the Cu(II)–F1S and Cd(II)–F1S, respectively. The decrease in the value of the band formed at 1645 cm^{-1} (stretching vibration of C=N) to 1620 cm^{-1} (in the case of copper adsorption) or 1630 cm^{-1} (in the case of cadmium adsorption) is evidence of complexation, as is shown in Scheme 3. The new bands at 473 cm^{-1} and 444 cm^{-1} are due to the stretching vibrations of the Cu-O and Cd-O, respectively.

Table 6. Comparison between the uptake capacity of the synthesized samples (F1 and F1S) and that of other adsorbents.

Adsorbent	Adsorption Capacity (mg/g)		Ref.
	Cd(II)	Cu(II)	
Chitosan/$MnFe_2O_4$ composite	9.73	43.94	[25]
Dithiocarbamate/Fe_3O_4/reduced graphene oxide composite	116.30	113.60	[26]
FAU zeolite	74.07	57.80	[27]
Calcium titanate	82.60	66.40	[28]
Silver/multiwalled carbon nanotubes	54.92	58.02	[29]
Guanyl-modified cellulose	68	83	[30]
F1	89.44	103.73	This study
F1S	155.04	177.94	This study



Scheme 3. The mechanism of removal of cadmium and copper ions using the F1 and F1S adsorbents.

The F1 adsorbent is characterized by the presence of negative charges that were neutralized by positive Na(I) ions due to the substitution of some divalent magnesium ions for some tetravalent silicon ions in the crystal lattice of the nanostructures. Subsequently, positive sodium ions can be exchanged by cadmium or copper ions, as is shown in Scheme 3. Figure 15A,B represents the EDX patterns of the Cu(II)–F1 and Cd(II)–F1, respectively. The success of the ion exchange mechanism of the F1 sample with Cu(II) ions is evident through the disappearance of sodium and the appearance of copper at 0.96 eV and 7.85 eV, as is shown in Figure 15A. The success of the ion exchange mechanism of the F1 sample with Cd(II) ions is evident through the disappearance of sodium and the appearance of cadmium at 3.04 eV, as is shown in Figure 15B.

3.2.5. Effect of Desorption and Reusability

Several eluting agents such as HCl, HNO_3, thiourea, and EDTA disodium salt were used, as is clarified in Figure 16. The results show that EDTA disodium salt achieved the highest % D. This increase in the removal rate when using EDTA disodium salt was obtained because EDTA has a greater affinity to form stable chelate complexes by reacting with aluminum ions [24]. The EDTA molecule has six potential sites for bonding with the aluminum ion (the four carboxylate groups and the two amino groups).

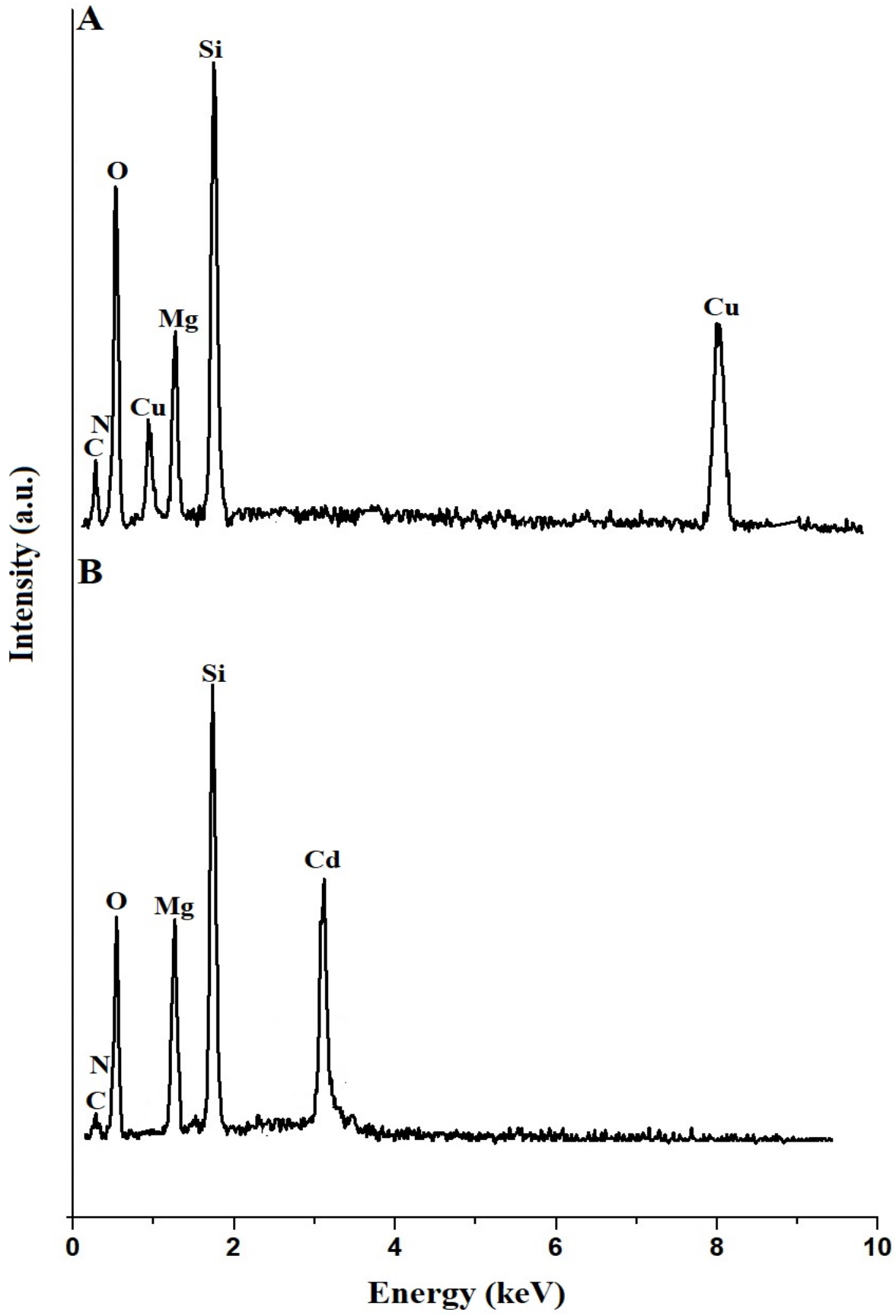


Figure 13. The EDX patterns of the Cu(II)–F1S (**A**) and Cd(II)–F1S (**B**).

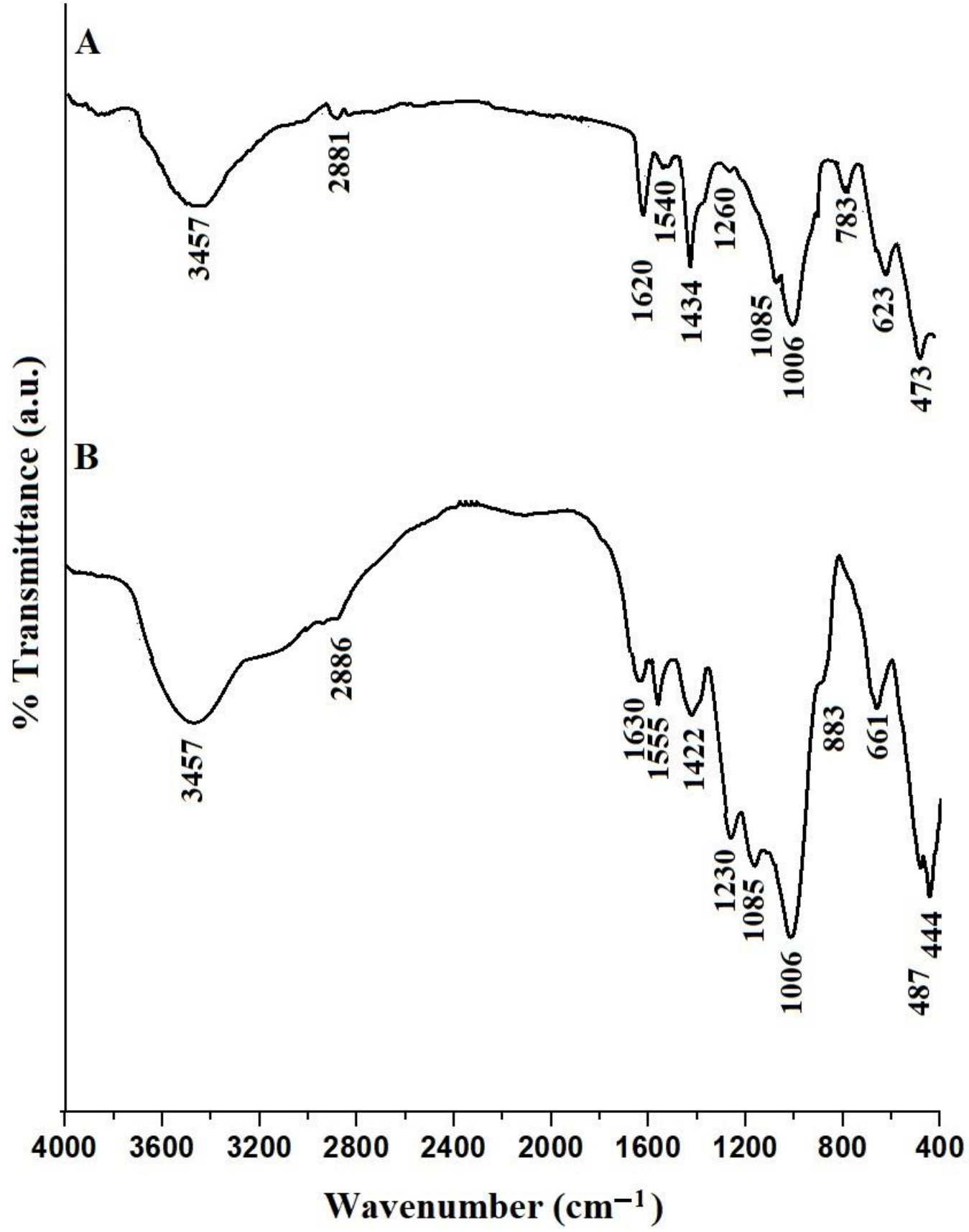


Figure 14. The FT-IR spectra of the Cu(II)–F1S (**A**) and Cd(II)–F1S (**B**).

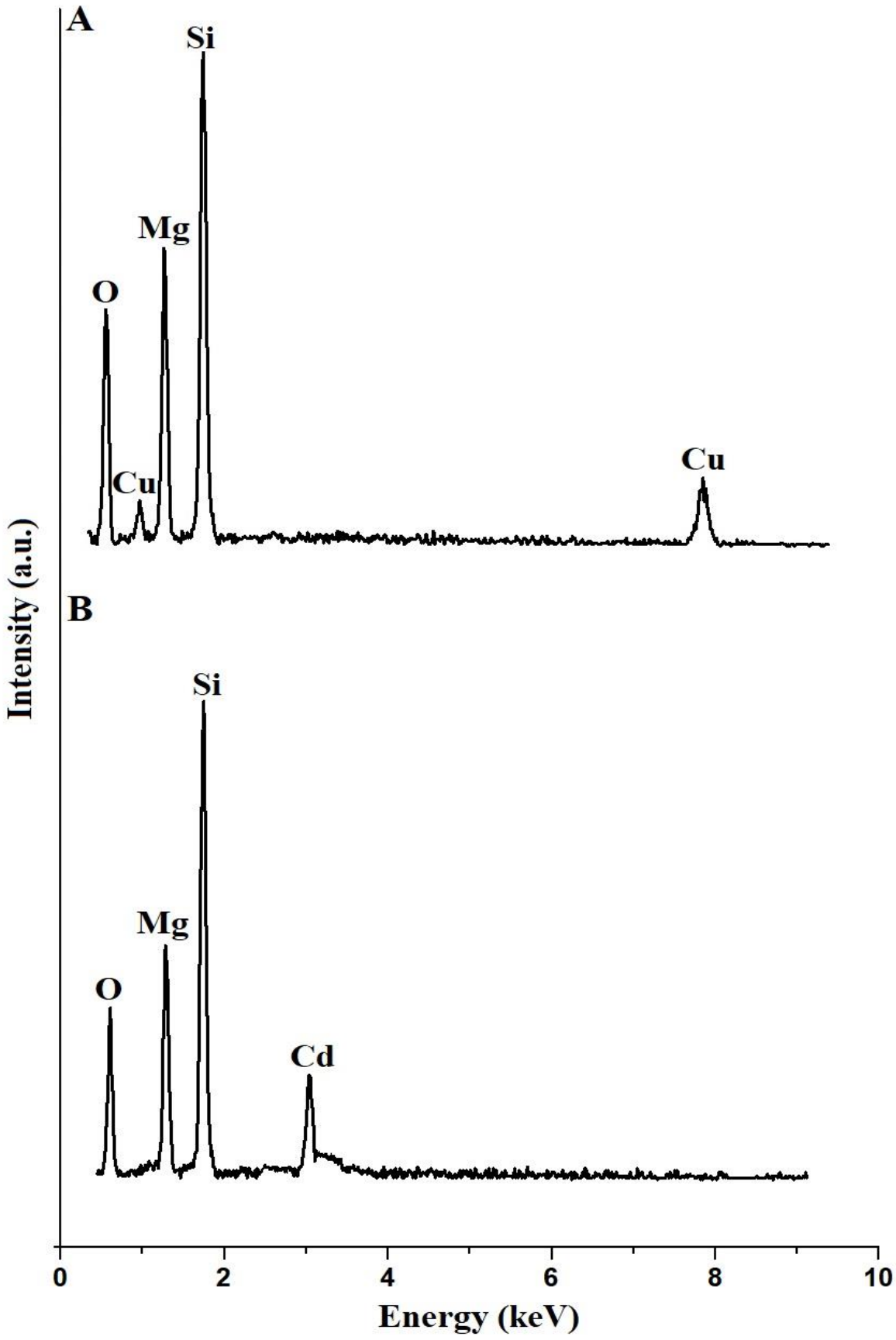


Figure 15. The EDX patterns of the Cu(II)–F1 (**A**) and Cd(II)–F1 (**B**).

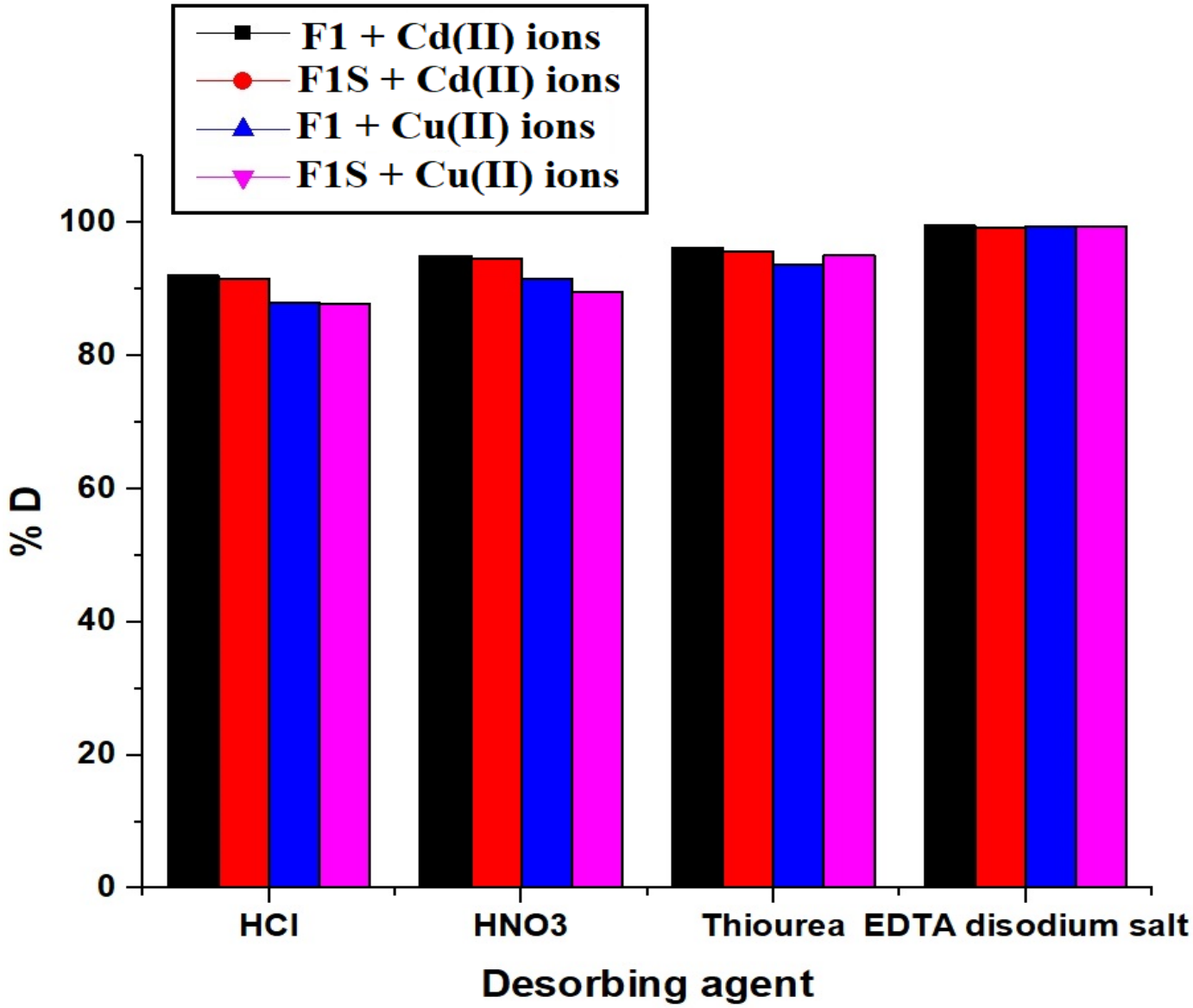


Figure 16. Desorption of copper and cadmium ions from the F1 and F1S samples using several eluting agents. Experimental conditions: concentration = 5 mg/L, volume of copper or cadmium solution = 40 mL, amount of adsorbent = 0.04 g, volume of eluting agent = 4 mL, temperature = 298 K, pH = 7.5, and time = 80 min.

Reusability experiments proved the possibility of using F1 and F1S samples to adsorb cadmium and copper ions five consecutive times without losing their efficiency, as is clarified in Figure 17.

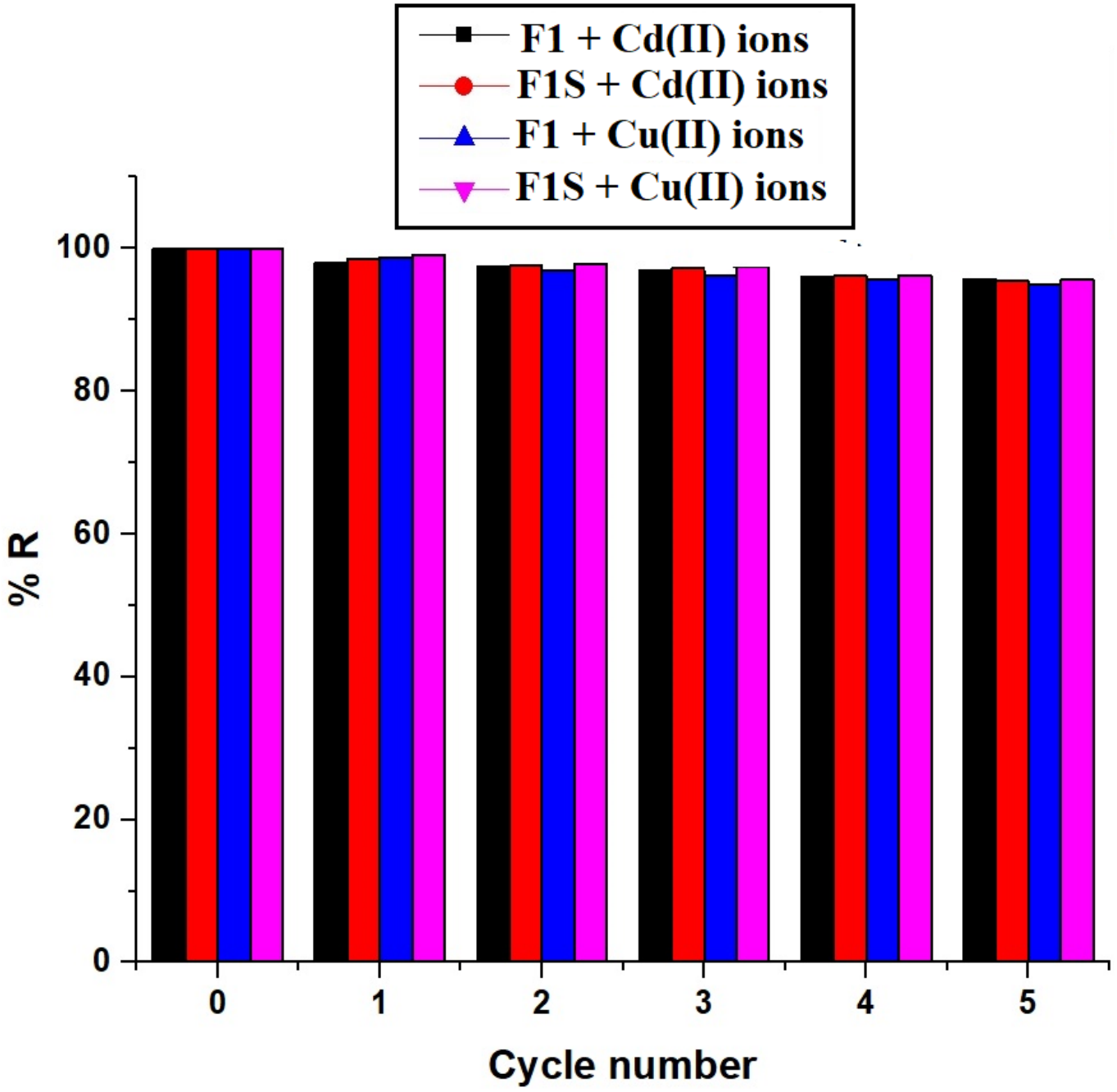


Figure 17. Reusability of the F1 and F1S samples for the adsorption of cadmium and copper ions. Experimental conditions: concentration = 5 mg/L, volume of Cd(II) or Cu(II) solution = 40 mL, amount of adsorbent = 0.04 g, volume of eluting agent = 4 mL, temperature = 298 K, pH = 7.5, and time = 80 min.

4. Conclusions

In this work, sodium magnesium silicate hydroxide/sodium magnesium silicate hydrate nanostructures were easily synthesized and then modified using 2,3-dihydroxybenzaldehyde as a novel nanocomposite. The anticipated decline in the surface area following the functionalization of the nanostructures with 2,3-dihydroxybenzaldehyde resulted from the presence of 2,3-dihydroxybenzaldehyde on the backbones of nanostructures, which prevents nitrogen gas from entering the pores of the nanostructures during the BET method. The morphology of the synthesized nanostructures changed from spheres, cubes, and irregular shapes to spherical conglomerates consisting of needle-like shapes due to func-

tionalization of the nanostructures with 2,3-dihydroxybenzaldehyde. The synthesized nanostructures and nanocomposite samples were used for the efficient removal of cadmium and copper ions from aqueous media using the ion exchange and chelation adsorption procedures, respectively. The synthesized nanostructures and nanocomposites are promising adsorbents in terms of their facile synthesis, low cost, and effectiveness. The factors affecting the adsorption process, such as pH, time, temperature, and concentration, were studied,. The maximum capacity of the synthesized nanostructures and nanocomposite samples to adsorb cadmium ions is 89.44 mg/g and 155.04 mg/g, respectively, and the maximum capacity of the synthesized nanostructures and nanocomposite samples to adsorb copper ions is 103.73 mg/g and 177.94 mg/g, respectively.

Author Contributions: Conceptualization, E.A.A.; methodology, E.A.A., E.S.A.-F. and A.S.A.-W.; software, M.T.B. and R.M.A.; formal analysis, A.S.A.-W.; investigation, A.S.A.-W., M.T.B. and R.M.A.; resources, E.A.A. and E.S.A.-F.; data curation, A.S.A.-W. and E.A.A.; writing—original draft A.S.A.-W., E.A.A., M.T.B. and R.M.A.; writing—review and editing, E.A.A., M.T.B. and R.M.A.; supervision, E.A.A.; project administration, A.S.A.-W.; funding acquisition, A.S.A.-W. All authors have read and agreed to the published version of the manuscript.

Funding: This research was funded by Princess Nourah bint Abdulrahman University Researchers Supporting Project number (PNURSP2023R35), Princess Nourah bint Abdulrahman University, Riyadh, Saudi Arabia.

Data Availability Statement: Not applicable.

Acknowledgments: The authors are grateful to Princess Nourah bint Abdulrahman University, Riyadh, Saudi Arabia for funding this work through Researchers Supporting Project number (PNURSP2023R35).

Conflicts of Interest: The authors declare no conflict of interest.

References

1. Xiang, H.; Min, X.; Tang, C.J.; Sillanpää, M.; Zhao, F. Recent Advances in Membrane Filtration for Heavy Metal Removal from Wastewater: A Mini Review. *J. Water Process Eng.* **2022**, *49*, 103023. [CrossRef]
2. Sinharoy, A.; Kumar, M.; Chaudhuri, R.; Saikia, S.; Pakshirajan, K. Simultaneous Removal of Selenite and Heavy Metals from Wastewater and Their Recovery as Nanoparticles Using an Inverse Fluidized Bed Bioreactor. *J. Clean. Prod.* **2022**, *376*, 134248. [CrossRef]
3. Yu, Y.; Zhong, Y.; Sun, W.; Xie, J.; Wang, M.; Guo, Z. A Novel Electrocoagulation Process with Centrifugal Electrodes for Wastewater Treatment: Electrochemical Behavior of Anode and Kinetics of Heavy Metal Removal. *Chemosphere* **2023**, *310*, 136862. [CrossRef]
4. Huang, H.; Li, Z.; Wang, H.; Xia, C.; Yan, P.; Zhang, Q.; Meng, Z. Adsorption Performance of Layered Double Hydroxides for Heavy Metals Removal in Soil with the Presence of Microplastics. *J. Environ. Chem. Eng.* **2022**, *10*, 108733. [CrossRef]
5. Ghamari, F.; Negar, Z.A.; Arjomandi, J.; Shi, H. Novel Polyaniline/8-Hydroxyquinoline Composite Electrode Materials for Simultaneous Electrochemical Removal of Heavy Metal Ions from Water Resources. *J. Environ. Chem. Eng.* **2022**, *10*, 108830. [CrossRef]
6. Zhao, S.; Zhao, M.; Fan, X.; Meng, Z.; Zhang, Q.; Lv, F. MoS42-Intercalated Magnetic Layered Double Hydroxides for Effective Removal and Expedient Recovery of Heavy Metals from Soil. *Chem. Eng. J.* **2023**, *454*, 139965. [CrossRef]
7. Mallik, A.K.; Kabir, S.F.; Bin Abdur Rahman, F.; Sakib, M.N.; Efty, S.S.; Rahman, M.M. Cu(II) Removal from Wastewater Using Chitosan-Based Adsorbents: A Review. *J. Environ. Chem. Eng.* **2022**, *10*, 108048. [CrossRef]
8. Lasheen, M.R.; Ammar, N.S.; Ibrahim, H.S. Adsorption/Desorption of Cd(II), Cu(II) and Pb(II) Using Chemically Modified Orange Peel: Equilibrium and Kinetic Studies. *Solid State Sci.* **2012**, *14*, 202–210. [CrossRef]
9. Chen, X.; Tong, A. Modification of Silica Nanoparticles with Fluorescein Hydrozide for Cu(II) Sensing. *Dyes Pigment.* **2012**, *95*, 776–783. [CrossRef]
10. Taseidifar, M.; Makavipour, F.; Pashley, R.M.; Rahman, A.F.M.M. Removal of Heavy Metal Ions from Water Using Ion Flotation. *Environ. Technol. Innov.* **2017**, *8*, 182–190. [CrossRef]
11. Chen, Q.; Yao, Y.; Li, X.; Lu, J.; Zhou, J.; Huang, Z. Comparison of Heavy Metal Removals from Aqueous Solutions by Chemical Precipitation and Characteristics of Precipitates. *J. Water Process Eng.* **2018**, *26*, 289–300. [CrossRef]
12. Cheng, X.; Zhang, Y.; Shao, S.; Lai, C.; Wu, D.; Xu, J.; Luo, X.; Xu, D.; Liang, H.; Zhu, X. Highly Permeable Positively Charged Nanofiltration Membranes with Multilayer Structures for Multiple Heavy Metal Removals. *Desalination* **2023**, *548*, 116266. [CrossRef]

13. Al-Wasidi, A.S.; Naglah, A.M.; Saad, F.A.; Abdelrahman, E.A. Modification of Sodium Aluminum Silicate Hydrate by Thioglycolic Acid as a New Composite Capable of Removing and Preconcentrating Pb(II), Cu(II), and Zn(II) Ions from Food and Water Samples. *Arab. J. Chem.* **2022**, *15*, 104178. [CrossRef]
14. Al-Wasidi, A.S.; AlSalem, H.S.; Alshalawi, A.F.; Naglah, A.M.; Al-Anwar, A.; Abdelrahman, E.A. Facile Synthesis of a Novel Nanocomposite for Determination of Mercury and Copper Ions in Food and Water Samples. *Arab. J. Chem.* **2022**, *15*, 104113. [CrossRef]
15. Al-Wasidi, A.S.; Naglah, A.M.; Saad, F.A.; Abdelrahman, E.A. Modification of Silica Nanoparticles with 1-Hydroxy-2-Acetonaphthone as a Novel Composite for the Efficient Removal of Ni(II), Cu(II), Zn(II), and Hg(II) Ions from Aqueous Media. *Arab. J. Chem.* **2022**, *15*, 104010. [CrossRef]
16. Abdelrahman, E.A.; Abou El-Reash, Y.G.; Youssef, H.M.; Kotp, Y.H.; Hegazey, R.M. Utilization of Rice Husk and Waste Aluminum Cans for the Synthesis of Some Nanosized Zeolite, Zeolite/Zeolite, and Geopolymer/Zeolite Products for the Efficient Removal of Co(II), Cu(II), and Zn(II) Ions from Aqueous Media. *J. Hazard. Mater.* **2021**, *401*, 123813. [CrossRef] [PubMed]
17. Abdelrahman, E.A.; Alharbi, A.; Subaihi, A.; Hameed, A.M.; Almutairi, M.A.; Algethami, F.K.; Youssef, H.M. Facile Fabrication of Novel Analcime/Sodium Aluminum Silicate Hydrate and Zeolite Y/Faujasite Mesoporous Nanocomposites for Efficient Removal of Cu(II) and Pb(II) Ions from Aqueous Media. *J. Mater. Res. Technol.* **2020**, *9*, 7900–7914. [CrossRef]
18. Gendy, E.A.; Ifthikar, J.; Ali, J.; Oyekunle, D.T.; Elkhlifia, Z.; Shahib, I.I.; Khodair, A.I.; Chen, Z. Removal of Heavy Metals by Covalent Organic Frameworks (COFs): A Review on Its Mechanism and Adsorption Properties. *J. Environ. Chem. Eng.* **2021**, *9*, 105687. [CrossRef]
19. Ren, Z.; Wang, L.; Li, Y.; Zha, J.; Tian, G.; Wang, F.; Zhang, H.; Liang, J. Synthesis of Zeolites by In-Situ Conversion of Geopolymers and Their Performance of Heavy Metal Ion Removal in Wastewater: A Review. *J. Clean. Prod.* **2022**, *349*, 131441. [CrossRef]
20. Azad, H.; Mohsennia, M.; Cheng, C.; Amini, A. Facile Fabrication of PVB-PVA Blend Polymer Nanocomposite for Simultaneous Removal of Heavy Metal Ions from Aqueous Solutions: Kinetic, Equilibrium, Reusability and Adsorption Mechanism. *J. Environ. Chem. Eng.* **2021**, *9*, 106214. [CrossRef]
21. Roy, A.; Bharadvaja, N. Efficient Removal of Heavy Metals from Artificial Wastewater Using Biochar. *Environ. Nanotechnol. Monit. Manag.* **2021**, *16*, 100602. [CrossRef]
22. Basu, H.; Saha, S.; Pimple, M.V.; Singhal, R.K. Novel Hybrid Material Humic Acid Impregnated Magnetic Chitosan Nano Particles for Decontamination of Uranium from Aquatic Environment. *J. Environ. Chem. Eng.* **2019**, *7*, 103110. [CrossRef]
23. Haripriyan, U.; Gopinath, K.P.; Arun, J. Chitosan Based Nano Adsorbents and Its Types for Heavy Metal Removal: A Mini Review. *Mater. Lett.* **2022**, *312*, 131670. [CrossRef]
24. Khalifa, M.E.; Abdelrahman, E.A.; Hassanien, M.M.; Ibrahim, W.A. Application of Mesoporous Silica Nanoparticles Modified with Dibenzoylmethane as a Novel Composite for Efficient Removal of Cd(II), Hg(II), and Cu(II) Ions from Aqueous Media. *J. Inorg. Organomet. Polym. Mater.* **2020**, *30*, 2182–2196. [CrossRef]
25. Li, H.; Ji, H.; Cui, X.; Che, X.; Zhang, Q.; Zhong, J.; Jin, R.; Wang, L.; Luo, Y. Kinetics, Thermodynamics, and Equilibrium of As(III), Cd(II), Cu(II) and Pb(II) Adsorption Using Porous Chitosan Bead-Supported $MnFe_2O_4$ Nanoparticles. *Int. J. Min. Sci. Technol.* **2021**, *31*, 1107–1115. [CrossRef]
26. Fu, W.; Huang, Z. Magnetic Dithiocarbamate Functionalized Reduced Graphene Oxide for the Removal of Cu(II), Cd(II), Pb(II), and Hg(II) Ions from Aqueous Solution: Synthesis, Adsorption, and Regeneration. *Chemosphere* **2018**, *209*, 449–456. [CrossRef]
27. Joseph, I.V.; Tosheva, L.; Doyle, A.M. Simultaneous Removal of Cd(II), Co(II), Cu(II), Pb(II), and Zn(II) Ions from Aqueous Solutions via Adsorption on FAU-Type Zeolites Prepared from Coal Fly Ash. *J. Environ. Chem. Eng.* **2020**, *8*, 103895. [CrossRef]
28. Hang, Y.; Si, Y.; Zhou, Q.; Yin, H.; Wang, A.; Cao, A. Morphology-Controlled Synthesis of Calcium Titanate Particles and Adsorption Kinetics, Isotherms, and Thermodynamics of Cd(II), Pb(II), and Cu(II) Cations. *J. Hazard. Mater.* **2019**, *380*, 120789. [CrossRef]
29. Ramana, D.K.V.; Yu, J.S.; Seshaiah, K. Silver Nanoparticles Deposited Multiwalled Carbon Nanotubes for Removal of Cu(II) and Cd(II) from Water: Surface, Kinetic, Equilibrium, and Thermal Adsorption Properties. *Chem. Eng. J.* **2013**, *223*, 806–815. [CrossRef]
30. Kenawy, I.M.; Hafez, M.A.H.; Ismail, M.A.; Hashem, M.A. Adsorption of Cu(II), Cd(II), Hg(II), Pb(II) and Zn(II) from Aqueous Single Metal Solutions by Guanyl-Modified Cellulose. *Int. J. Biol. Macromol.* **2018**, *107*, 1538–1549. [CrossRef]

Disclaimer/Publisher's Note: The statements, opinions and data contained in all publications are solely those of the individual author(s) and contributor(s) and not of MDPI and/or the editor(s). MDPI and/or the editor(s) disclaim responsibility for any injury to people or property resulting from any ideas, methods, instructions or products referred to in the content.